



Gesellschaft für Reaktorsicherheit (GRS) mbH

A NONLINEAR 3D REAL-TIME MODEL
FOR SIMULATION OF BWR NUCLEAR
POWER PLANTS

Y. Ercan



Gesellschaft für Reaktorsicherheit (GRS) mbH

A NONLINEAR 3D REAL-TIME MODEL
FOR SIMULATION OF BWR NUCLEAR
POWER PLANTS

Yücel Ercan

Visiting professor from the
Middle East Technical University,
Ankara, Turkey

GRS-42 (Februar 1982)

Schwertnergasse 1 · 5000 Köln 1 · Telefon (02 21) 20 68-0 · Telex 8 881 807 grs d

Keywords/Deskriptoren

Real-Time - Simulator - Boiling Water Reactor (BWR) - Process
Computer - Core Surveillance - Core Model - Plant Model -
Neutron Kinetics - Thermodynamics - Hydrodynamics

Acknowledgement

This work has been greatly supported by the Alexander von Humboldt Foundation of the Federal Republic of Germany and the Gesellschaft für Reaktorsicherheit (GRS) mbH as host institute to the author. The author acknowledges gratefully their helpfulness.

He wishes also to express his sincere thanks to Dr. A. Hoeld and Dr. O. Lupas for their valuable suggestions, close collaboration, and for their understanding in allowing him to use the results and subroutines of the code GARLIC.

Thanks are due also to the other GRS personnel for their efforts during different phases of the work.

Abstract

A nonlinear transient model for BWR nuclear power plants which consist of a 3D-core (subdivided into a number of superboxes, and with parallel flow and subcooled boiling), a top plenum, steam removal and feed water systems and main coolant recirculation pumps is given. The model describes the local core and global plant transient situation as dependent on both the inherent core dynamics and external control actions, i.e., disturbances such as motions of control rod banks, changes of mass flow rates of coolant, feed water and steam outlet. The case of a pressure- controlled reactor operation is also considered.

The model which forms the basis for the digital code GARLIC-B (Er et al. 82) is aimed to be used on an on-site process computer in parallel to the actual reactor process (or even in predictive mode). Thus, special measures had to be taken into account in order to increase the computational speed and reduce the necessary computer storage. This could be achieved by

- separating the neutron and power kinetics from the xenon-iodine dynamics,
- treating the neutron kinetics and most of the thermodynamics and hydrodynamics in a pseudostationary way,
- developing a special coupling coefficient concept to describe the neutron diffusion, calculating the coupling coefficients from a basic neutron kinetics code,
- combining coarse mesh elements into superboxes, taking advantage of the symmetry properties of the core and
- applying a sparse matrix technique for solving the resulting algebraic power equation system.

Kurzfassung

Beschrieben wird ein nichtlineares Transientenmodell für SWR-Kernenergieanlagen, die sich zusammensetzen aus einem 3dimensionalen Kern, einem oberen Plenum, einem Frischdampf- und ei-

nem Speisewassersystem sowie einem Fallraum mit Kühlmittelumwälzpumpen. Der Kern ist unterteilt in eine Anzahl von Superboxen und Parallelkanälen, in denen Kühlmittel mit unterschiedlicher Geschwindigkeit nach oben strömt (unterkühltes Sieden muß in Betracht gezogen werden). Das Programm berechnet das transiente Verhalten der lokalen und globalen Kern- und Anlagenparameter in Abhängigkeit sowohl von der inhärenten Kerndynamik als auch von Eingriffen von außen, wie z.B. Bewegungen der Regelstabbänke sowie Störungen in den Massenströmen der Hauptkühlmittelpumpe, des Speisewassers und der Dampfentnahme. Ein druck geregelter Reaktorbetrieb kann ebenfalls simuliert werden.

Das Modell bildet die Grundlage für das Rechenprogramm GARLIC-B. Dieses Programm soll auf einer im Reaktorgebäude befindlichen Prozeßrechneranlage ablauffähig sein, wobei der tatsächliche Prozeßverlauf im Reaktor entweder parallel oder sogar in prädiktiver Weise nachgerechnet werden soll. Die dadurch bedingten speziellen Anforderungen an das Verfahren, vor allem bezüglich schnellerer Rechenzeiten und Einsparungsmöglichkeiten im Speicherplatzbedarf, konnten erreicht werden durch

- Separation der Neutronen- bzw. Leistungskinetik von der Xenon-Jod-Dynamik,
- pseudostationäre Behandlung der Neutronenkinetik und Thermo- und Hydrodynamik,
- Einsatz eines Kopplungskoeffizientenkonzepts für die Darstellung der Neutronendiffusion, bei dem die Kopplungskoeffizienten aus Startrechnungen mit einem Basis-Neutronenkinetik-Code bestimmt werden,
- Zusammenfassen von Grobgitterboxen des Kerns in Superboxen, wobei gleichzeitig die Vorteile der Symmetrieeigenschaften des Kerns nutzbar gemacht werden können, und
- Lösung der resultierenden algebraischen Leistungsdichtegleichungen mit Hilfe einer Sparse-Matrix-Technik.

Contents

	page
1. Introduction	1
2. Neutron Kinetics	5
2.1 Basic Equations	5
2.2 Macroscopic Cross Sections	6
2.3 Control Rod Movement	8
2.4 Spatial Coupling Coefficients	9
2.5 1 1/2 Group Representation	11
2.6 Homogenization (Superbox Representation)	13
3. Thermo- and Hydrodynamic Core and Plant Parameters	17
3.1 Core Nodal Structure	17
3.2 Nodal Coolant Mass Flow Rate	19
3.3 Steam Quality and Void Fraction	19
3.3.1 Location of Bubble Detachment Point	21
3.3.2 Steam Quality and Void Fraction Distributions for the Transient Case	24
3.3.2.1 Case A: Channels without Border Zone	26
3.3.2.2 Case B: Channels with Border Zone	28
3.3.3 Steam Quality and Void Fraction Distribution at Working Point	34
3.4 Coolant Mass Flow Distribution	34
3.5 Nodal Coolant Temperature Distribution	38
3.5.1 Transient Calculations	38
3.5.1.1 Channels without Border Zone	38
3.5.1.2 Channels with Border Zone	45
3.5.2 Calculations at the Working Point	51
3.6 Nodal Fuel Temperature Distribution	52
3.7 System Pressure	53
3.8 Water Level in Top Plenum	55
3.9 Feed Water and Outlet Steam Flow Rates and Water Volume in Top Plenum when Pressure is Controlled (Water Level is Constant)	58

3.9.1	Feed Water and Outlet Steam Flows are not Prescribed	58
3.9.2	Externally Prescribed Feedwater and Outlet Steam Flows	60
3.10	Thermodynamic Properties	61
4.	Xenon-Iodine Distribution	62
5.	Modification of Power Density Distribution Equation	63
5.1	Power Feedback from the Coolant Temperature Term	63
5.2	Power Feedback from the Fuel Temperature Term	64
5.3	Power Feedback from the Void Fraction Term	66
5.4	Modification of the Power Matrix	67
6.	Results of Preliminary Tests	71
6.1	The Computer Code GARLIC-B	71
6.2	Preliminary Tests Results	72
7.	Final Remarks	72
	References	80
Appendix 1:	The Power Feedback Coefficients from the Coolant Temperature Terms	
Appendix 2:	The Power Feedback Coefficients from the Void Fraction Terms	

Figures

	page
1.1: Schematic Diagram of a BWR Core	2
3.1: Numbering Convention on a Nodal Column	18
3.2: Depiction of the Need for a Border Zone	22
3.3: Construction of a Border Zone	23
3.4: Channel with Border Zone. Bubble Detachment Point (C) is in Node n_1	28
3.5: Channel with Border Zone. Bubble Detachment Point (C) in Node n_1+1	32
3.6: Channel without Border Zone. Node with Bubble Detachment Point (C), without Boiling Boundary	40
3.7: Channel without Border Zone. Node with Bubble Detachment Point (C) and with Boiling Boundary (D)	42
3.8: Channel without Border Zone. Node with Sub- cooled Boiling, without Bubble Detachment Point and without Boiling Boundary	43
3.9: Channel without Border Zone. Node with Sub- cooled Boiling, without Bubble Detachment Point and with Boiling Boundary (D)	44
3.10: Channel with Border Zone. Node with Sub- cooled Boiling. Bubble Detachment Point (C) in Node n_1+1	46
3.11: Channel with Border Zone. Node with Sub- cooled Boiling. Bubble Detachment Point (C) in Node n_1 . Temperature Profile in Node n_1	49
3.12: Channel with Border Zone. Node with Sub- cooled Boiling. Bubble Detachment Point (C) in Node n_1 . Temperature Profile in Node n_1+1	50
3.13: Model of the Top Plenum	54
6.1: Transient Behavior of a BWR Nuclear Power Plant; Coolant Mass Flow Changed (System Pressure Control, 1/4 Core, 16 Nodes)	73
6.2: Transient Behavior of a BWR Nuclear Power Plant; Control Rod Bank 9 Moved (System Pressure Control, 1/4 Core, 16 Nodes)	74
6.3: Transient Behavior of a BWR Nuclear Power Plant; Feed Water Temperature Changed (Sys- tem Pressure Control, 1/4 Core, 16 Nodes)	75

6.4:	Transient Behavior of a BWR Nuclear Power Plant; Coolant Mass Flow Changed (System Pressure Free, 1/4 Core, 96 Nodes)	76
6.5:	Transient Behavior of a BWR Nuclear Power Plant; Control Rod Bank 9 Moved (System Pressure Free, 1/4 Core, 96 Nodes)	77

Tables

6.1:	Computational Information about the Test Runs	78
------	---	----

Nomenclature

A_k	net flow area of the k'th nodal column
A_{ko}	inlet orifice area of the k'th nodal column
A_r	ratio of net flow area to total area of a nodal column
A_T	free water surface area in top plenum
A_{tk}	total area of the k'th nodal column
$B(x,p)$	Bankoff two-phase correlation
C_d	discharge coefficient
C_λ^T	constant in eq. 3.111
C_{inr}	homogenizing rod factor
D_{1n}	diffusion constant
D_{2n}	diffusion constant
D_{A2nw}	coefficient in eq. (2.40) as defined in (Er 80)
D_{12nw}	coefficient in eq. (2.40) as defined in (Er 80)
D_{F1nw}	coefficient in eq. (2.40) as defined in (Er 80)
D_{F2nw}	coefficient in eq. (2.40) as defined in (Er 80)
d_H	hydraulic diameter
E_{eff}	energy conversion factor
G_E	total coolant mass flow rate into core
G_{FW}	feed water flow rate
G_k	coolant mass flow rate through the k'th nodal column
G_{SH}	saturated steam flow rate into top plenum
G_{ST}	outlet steam flow rate from top plenum
G_{WDE}	flow rate through downcomer
G_{WH}	saturated water flow rate into top plenum
g	gravitational acceleration
h	specific enthalpy
h'	specific enthalpy of saturated water

h''	specific enthalpy of saturated steam
h_{dL}	specific enthalpy at bubble detachment point
h_{sw}	latent heat, $h''-h'$
h_w	specific enthalpy of liquid water
I	iodine density
J_{inm}	neutron current density from node n in direction of neighbor n_m (through surface σ_{nm})
k_f	thermal conductivity of liquid water
M_n	total number of neighboring nodes
N	total number of nodes
Nu	Nusselt number
n_{bk}	boiling index
n_{dk}	bubble detachment index
n_{xy}	total number of nodal columns
n_z	total number of node layers
n_1, n_1+1	indices of nodes which carry border zone
P	power density
Pe	Peclet number
p	system pressure
p_{cn}	nodal pressure
p_{zn}	dp/dz in nodal columns
q	heat flux
R	total number of control rod banks
r_a	fuel rod radius
r_{ca}	outer radius of canning
r_{ci}	inner radius of canning
r_k	fluid resistance at the inlet of the k 'th nodal column
S	slip ratio in two-phase flow
S_f	fuel rod periphery per unit flow area

St	Stanton number
T	temperature
T_{cn}	coolant water bulk temperature
T_{CN}	normalization value for coolant temperature
T_E	water temperature at core entrance
T_{Fc}	fuel rod canning temperature
T_{Fn}	fuel rod temperature
T_{FN}	normalization value for fuel rod temperature
T_{Fs}	fuel rod surface temperature
T_s	water saturation temperature
T_w	water temperature (of liquid phase)
t	time
t_w	time at working point
U_{nr}	movement of rod bank r in node n
U_{Nr}	normalization value for rod bank movement
V	volume, fluid mass velocity (kg/m^2 -sec)
V_T	total top plenum volume
V_{WT}	water volume in top plenum
Xe_n	nodal xenon density
Xe_N	normalization value for xenon density
x	thermodynamic steam quality
x_d	thermodynamic steam quality at the bubble detachment point
x_T	average steam quality at the top plenum
x_t	true steam quality
z, z'	distance along node column
z_{bk}	distance of boiling boundary to core entrance
z_{dk}	distance of bubble detachment point to core entrance
z_H	total length of nodal column

z_{WL}	water level in top plenum
z_{xk}	distance of bubble detachment point to border zone entrance
α	void fraction, heat transfer coefficient
α_{cn}	nodal overall heat transfer coefficient from inner surface of canning to the coolant
α_{Fn}	nodal overall heat transfer coefficient from fuel surface through gap and canning to the coolant
α_G	nodal overall heat transfer coefficient from fuel surface through gap to canning inner surface
α_N	normalization value for void fraction
α_n	nodal void fraction
α_{wcn}	nodal heat transfer coefficient from outer surface of canning to the coolant
Γ	xenon absorption factor
γ_I	iodine fission yield
γ_T	average void fraction in top plenum
γ_X	xenon fission yield
Δp_A	acceleration pressure drop along a nodal column
Δp_F	friction pressure drop along a nodal column
Δp_I	inlet throttling pressure drop
Δp_k	total pressure drop along the k'th nodal column
Δp_S	static pressure drop along a nodal column
ΔT_d	subcooling at bubble detachment point
Δz^-	border zone width
Δz_{bk}	distance of boiling boundary to node entrance
Δz_{dk}	distance of bubble detachment point to node entrance
Δz_n	axial height of node n

$\delta_{..}$	absolute deviation from working point
$\delta_{r..}$	normalized deviation from working point
$\delta_{n_m, n}$	Kronocker symbol meaning only two neighboring nodes n and n_m contribute to calculations of nondiagonal coupling coefficients
ϵ_F	percentage heat power lost in γ radiation
ϵ_n	fast fission factor
ϵ_{VF}	fuel volume fraction within the core (canning not included)
η_n	term defined by eq. (2.31)
λ_{BFR}	Darcy-Weisbach friction factor for boiling region
λ_C	heat conduction coefficient in canning
λ_F	heat conduction coefficient in fuel rod
λ_{FC}	constant in eq. (3.111)
λ_I	iodine decay constant
λ_{NFR}	Darcy-Weisbach friction factor for nonboiling region
λ_x	xenon decay constant
$\nu_1 = \nu_2 = \nu$	number of neutrons (fast and thermal) per fission
ρ	mass density
ρ'	liquid water density at saturation state
ρ''	steam density at saturation state
ρ_w	liquid water density
σ_{nm}	surface area of node n (in direction of node n_m)
Σ_{a1}	absorption cross-section for fast neutron energy group
Σ_{a2}	absorption cross-section for slow neutron energy group
Σ_{f1}	fission cross-section for fast neutron energy group
Σ_{f2}	fission cross-section for slow neutron energy group
Σ_{12}	slowing down cross-section
Σ_{al}^{FR}	absorption cross-section at reference fuel temperature (fast neutrons)

Σ_{L2n}	thermal leakage term
ϕ_{1n}	nodal flux (averaged over node n) for the fast neutron group
ϕ_{2n}	nodal flux (averaged over node n) for the slow neutron group
$\phi(x_n, p)$	Martinelli-Nelson two-phase friction pressure gradient multiplier
w_{in}	diagonal coupling coefficient
w_{inm}	non-diagonal coupling coefficient
w_n	modified diagonal coupling coefficient
w_{nm}	modified nondiagonal coupling coefficient

Subscripts

a	absorption
b	boiling boundary
B	beginning of time step
BM	average in boiling part of a node
Bz	border zone
c	coolant
CR	coolant reference temperature
e	exit
E	core entrance
f	fission
F	fuel, end of time step
Fs	fuel surface
FR	at fuel reference temperature
h	basic volume element
i	inlet

k	nodal column of index k
n	node of index n
n_m, nm	neighboring node of index n_m
N	normalizing quantity
NBz	outside of border zone
r	normalized
w	working point, water
l2	slowing down

Superscripts

C	derivative with respect to coolant temperature
CR	coolant reference temperature
D	derivative with respect to density
F	derivative with respect to fuel temperature
FR	fuel reference temperature
T	derivative with respect to temperature
x	derivative with respect to xenon density
α	derivative with respect to void fraction
'	saturated water
"	saturated steam

1. INTRODUCTION

The energy crisis which the world has been experiencing since 1973 will eventually increase the share of nuclear power plants in producing electrical energy. Especially, those developed countries which produce no oil may have to lean on nuclear energy heavily in the coming decades. As the production of nuclear energy increases, nuclear power plants will have to be used not only as constant power producing base energy sources but also as variable power producing sources which follow the changing energy demand of the electric network. As a result, increasing attention has been paid to the surveillance and control of large nuclear reactor cores recently. Theoretical models and codes which simulate the transient behavior of nuclear power plants with reasonable speed and memory capacity have become of interest because of their potential uses in the on-line, real-time applications (for reactor surveillance, state prediction and control) as well as in operator training and in off-line simulations of the core and plant dynamics.

"Gesellschaft für Reaktorsicherheit (GRS) mbH" has been actively involved in the field of core surveillance and control. A real time, non-linear core and plant model (Ho, Lu 80; Ho, Lu 81; Ho, Lu 82) for simulation of PWR nuclear power plants and the corresponding computer code GARLIC (Ho et al. 82) have been developed within the framework of the project "Core Surveillance" (Ho et al. 81). In addition, a core power distribution method which is based on hierarchical control techniques has been formulated and incorporated into a digital control code MCCS (Be et al. 80; Be 83).

The study which is presented in this report was initiated later (at the beginning of 1980) with the support of the Alexander von Humboldt Foundation (Bonn). The purpose of the study is to develop an analogous model to simulate in real-time the transient behaviours of the nodal BWR core and global plant parameters. The model forms the basis for the digital code GARLIC-B (Er et al. 81) which is being tested at GRS at the present time.

The plant which is considered by the model consists of a core, a top plenum, main steam and feed water systems as well as main coolant circulation pumps (see fig. 1.1). It may be disturbed externally by a movement of control rod banks, or by changes in main coolant flow, feed water flow, feed water temperatures and outlet steam flow.

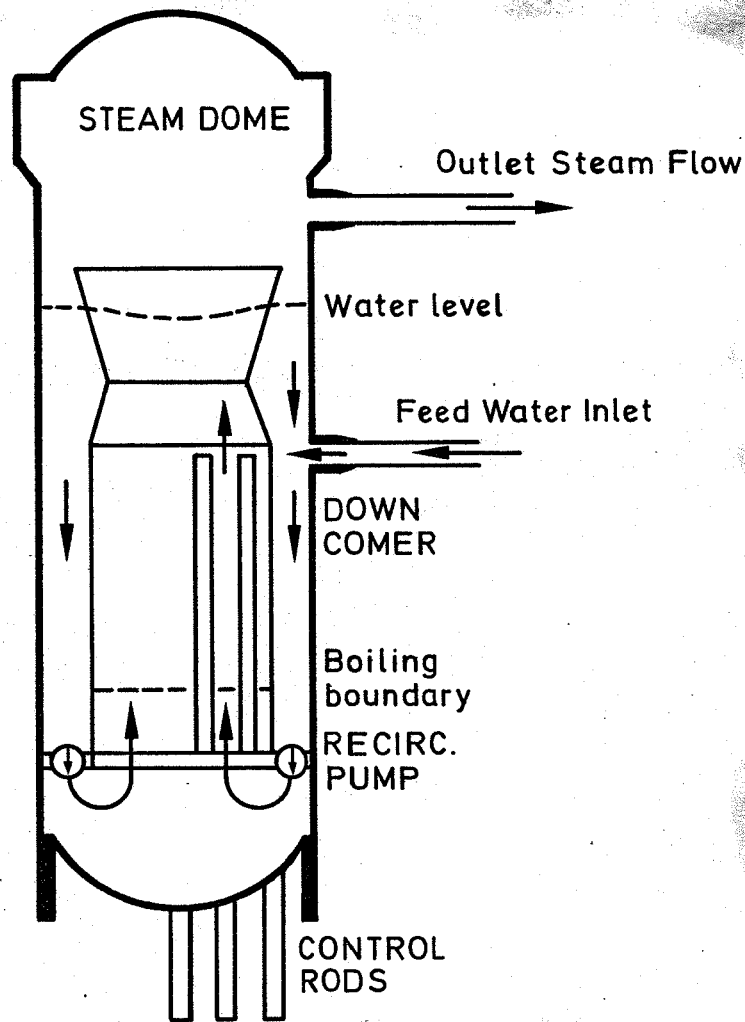


Figure 1.1:
Schematic Diagram of a BWR Core

Since the BWR model which is presented here was developed in parallel to, but later than the PWR model of GARLIC (Ho, Lu 80; Ho, Lu 81; Ho et al. 82), the past experience accumulated from

development of GARLIC could be used directly. Therefore, the assumptions dealing with the neutron kinetics and some concerning the thermo-hydrodynamics (e.g., those related to the calculation of fuel temperature distribution) are the same as in GARLIC. For the present BWR model, obviously a number of new assumptions have been made. Different methods have been developed to describe most of the thermo-hydrodynamic parameters and to calculate the transient behavior of the total plant.

The main features of the model are summarized below:

- The model describes the transient behavior of the characteristic local core as well as global plant parameters.
- The neutron kinetics, most of the thermo- and hydrodynamic calculations and xenon-iodine dynamics are decoupled from each other, calculated separately, and then combined into a total system by a recursive procedure.
- The application of the code is restricted to the normal operational transients, i.e., to not-too-fast varying perturbation signals. Thus, the neutron kinetics and most of the thermo- and hydrodynamics are treated as pseudo-stationary.
- The core is divided into coarse mesh volume elements and the neutron interactions between the neighboring volume elements are described by means of spatial coupling coefficients. As a result, the original pseudo-stationary diffusion equation is reduced to a set of algebraic equations. The coupling coefficients are evaluated by using the current density, flux, power density and cross-section values (at a working time point) from more comprehensive codes (such as QUABOX/CUBBOX (La et al. 77a; La et al. 77b; La et al. 78), ABCBOX (Fi,Fi 81), IQSBOX (Fi,Gu 81; Lo et al. 81)) which solve the neutron diffusion equations in a direct manner.
- Two-group neutron kinetic representation is reduced to 1 1/2 group by replacing the neutron flux terms by power density expressions and introducing modified coupling coefficients.
- Coarse mesh elements are combined into superboxes (nodes) by homogenizing the related core parameters and by calculating

a new set of coupling coefficients using a suitable rebalancing method (Si 76). Due to their special form of definitions, these coupling coefficients are expected to stay almost constant throughout different transient conditions.

- Sparse matrix techniques (AT 80) are used to solve the power density values from the algebraic set of equations, thus allowing savings in computer time and capacity.
- Calculations may be carried out for full, half, quarter or one-eighth core if the full core is suitably symmetrical. (Rotational symmetry is also included.) The core may be rectangular or jagged. Superboxes may be regular (each superbox is a parallel epiped with six neighbours) or non-regular (parallel epiped with more or less than six neighbours). Only the fuel region is divided into nodes. The influence of a reflector zone on a neighboring node is taken into account by corrected coupling coefficients.
- In general, nonlinear equations were used as a basis for the transient calculations of the neutron kinetics, xenon-iodine densities as well as thermo-hydraulic parameters.
- Because of the pseudo-stationary assumption, the spatial changes in the coolant flow rate along any channel can be neglected, i.e., the local coolant flow rate is equal to its entrance value. To determine the flow distribution at the core inlet, the total pressure drops are calculated along all channels for an initial flow distribution which is then modified recursively until the pressure drops over the whole length of all channels are equal to each other and the sum of the flows through the channels are equal to the total core flow.
- Since the coolant density changes which arise from void fraction variations affect the core power very strongly in a BWR, nodal steam quality values are determined by taking into account also subcooled boiling effects within a channel. The point of net vapor generation is found by using the Saha and Zuber correlation (Sa,Zu 74). In adaptation of this correlation to the superbox model, some extra precautions had to

be taken. Steam quality calculations are repeated at each time step during transient calculations. The flashing and condensation effects resulting from system pressure changes are included in the equations.

- Nodal void fraction values are calculated from the nodal steam qualities and the system pressure by using the Bankoff (Ba 60) two-phase correlation.
- Coolant temperature distribution is determined by distinguishing between non-boiling, subcooled boiling and bulk boiling regions.
- For fuel temperature calculations temperature dependent heat conduction coefficients are assumed. At present, only two separate overall heat transfer coefficients are used, one for the one-phase and one for the two-phase flow region.
- System pressure, water level and water volume within the top plenum are calculated by assuming uniform two-phase mixture within the top plenum and using non-stationary equations. Flashing and condensation effects are taken into account.
- The system may be disturbed by motions of control rod banks and/or changes in coolant mass flow rate, feed water mass flow rate, feed water temperature and outlet steam mass flow rate. In addition, in order to describe a pressure controlled reactor, the system pressure may be free or forced to follow a given function in time while keeping the water level in the top plenum constant.

2. NEUTRON KINETICS¹⁾

2.1 Basic Equations

Assuming two-energy groups of prompt neutrons (i.e., the fast and thermal neutron fluxes ϕ_1 and ϕ_2) the general neutron kinet-

¹⁾ This section is taken from (Ho, Lu 81) and adapted to BWR by the author by introducing the terms which involve void fraction. Full credit is given to A. Hoeld and O. Lupas.

ics representation is governed in case of a pseudo-stationary situation by the neutron diffusion equations of the form

$$D_1 \nabla^2 \phi_1 - (\Sigma_{a1} + \Sigma_{12}) \phi_1 + \frac{v}{k} (\Sigma_{f1} \phi_1 + \Sigma_{f2} \phi_2) = 0 \quad (2.1)$$

$$D_2 \nabla^2 \phi_2 - \Sigma_{a2} \phi_2 + \Sigma_{12} \phi_1 = 0 \quad (2.2)$$

(∇^2 = Laplace operator)

The boundary conditions follow from the continuity conditions, relating the flux gradients and the current densities \vec{J}_i as given by Fick's law.

2.2 Macroscopic Cross Sections

The macroscopic absorption, fission and slowing down cross sections (marked by the indices a, f and 12) averaged over a volume element n are dependent on different local BWR-core parameters, such as void fraction α_n , fuel rod temperature T_{Fn} , moderator temperature T_{Wn} (influencing them both directly and through a change in moderator density ρ_{Wn}), xenon density Xe_n and the insertion depth U_{nr} of the different control rod banks r ($r=1, \dots, R$). Knowing the macroscopic cross section values at the working point t_w their transient behaviour can then be represented as a function of the deviations of these parameters from their working point values. The fission cross sections can for example be represented as

$$\Sigma_{fin} = \Sigma_{finw} + \Sigma_{fin}^F \delta T_{fn} + \Sigma_{fin}^C \delta T_{Cn} + \sum_{r=1}^R (\Sigma_{finr}^U \delta U_{nr}) + \Sigma_{vin}^D \rho_{Cn}^\alpha \delta \alpha_n$$

(i=1,2; n=1, \dots, N) \quad (2.3)

Similar relations for the absorption and the slowing down cross sections can be established.

The dependency of the nodal macroscopic cross sections on their fuel rod temperature can be expressed by the relation

$$\Sigma_{ain}(T_{Fn}) = \Sigma_{ai}^{FR} [1 + \gamma_{ai}^{FR} (\sqrt{T_{Fn} + 273.15} - \sqrt{T_{FR} + 273.15})]$$

(i=1,2; n=1,...,N) (2.4)

with the corresponding macroscopic cross section Σ_{ai}^{FR} and the constant γ_{ai}^{FR} at a reference temperature T_{FR} , i.e.

$$\Sigma_{ain}(T_{Fn}) = \Sigma_{ainw} + \gamma_{ai}^{FR} \Sigma_{ai}^{FR} (\sqrt{T_{Fn} + 273.15} - \sqrt{T_{FR} + 273.15})$$

(i=1,2; n=1,...,N) (2.5)

Then, the derivative term Σ_{ain}^F is obtained as a function of fuel temperature from eq. (2.5) as

$$\Sigma_{ain}^F = 0.5 \gamma_{ai}^{FR} \Sigma_{ai}^{FR} / \sqrt{T_{Fn} + 273.15} = 0.5 \epsilon_{3ai}^{FR} \sqrt{T_{Fn} + 273.15}$$

(i=1,2; n=1,...,N) (2.6)

from which Σ_{ainw}^F is obtained as a special case by substituting $T_{Fn} = T_{Fnw}$. Similar relations are valid also for the cases Σ_{fin}^F and Σ_{12n}^F .

A change in water density as a result of a change in water temperature affects indirectly the macroscopic cross sections, characterized by the relation

$$\Sigma_{ain}(\rho_{wn}) = \Sigma_{ai}^{CR} + \epsilon_{1ai}^{CR} (\rho_{wn} - \rho_{wR}) + \epsilon_{2ai}^{CR} (\rho_{wn} - \rho_{wR})^2$$

(i=1,2; n=1,...,N) (2.7)

with the corresponding macroscopic cross section Σ_{ai}^{CR} and the constants ϵ_{1ai}^{CR} , ϵ_{2ai}^{CR} given at the reference water temperature T_{CR} .

Then, the derivative term Σ_{ain}^D is obtained from eq. (2.7) as

$$\Sigma_{ain}^D = \epsilon_{1ai}^{CR} + 2\epsilon_{2ai}^{CR} (\rho_{wn} - \rho_{wR})$$

(i=1,2; n=1,...,N) (2.8)

but

$$\rho_{wN} - \rho_{wR} = \rho_w^T (T_{Cn} - T_{CR}) \quad (2.9)$$

hence,

$$\Sigma_{ain}^D = \varepsilon_{1ai}^{CR} + 2\varepsilon_{2ai}^{CR} (T_{Cn} - T_{CR}) \rho_w^T \quad (2.10)$$

from which Σ_{ainw}^D is obtained by substituting $T_{Cn} = T_{Cnw}$.

Again similar relations for the corresponding cases Σ_{fin}^D and Σ_{12n}^D can be established.

The other derivatives of the macroscopic cross sections, e.g. with respect to the (direct) influence of the moderator temperature and xenon density can be considered to be constant. That is,

$$\Sigma_{ain}^M = \Sigma_{aiw}^M \quad (2.11)$$

and

$$\Sigma_{ain}^X = \Sigma_{aiw}^X \quad (i=1,2; n=1,\dots,N) \quad (2.12)$$

2.3 Control Rod Movement

Other than the coolant flow rate, which is the main power control mechanism in a BWR, the power density distribution can be affected by a variation in the insertion depth of the R different control rods or banks.

From the knowledge of the x-y position of each member of the controller r and the corresponding insertion depth U_r of the rod, the absolute and the relative nodal movement of the corresponding rod ends $(\delta U_{nr}, \delta_r U_{nr})$ of the control rod bank r within each node n can be determined (see again (Ho, Lu 81)).

2.4 Spatial Coupling Coefficients

The balance between the out- and ingoing neutron net current density terms over a node n (with a surface σ_n) is given by the equation

$$\int_{V_n} D_i \nabla^2 \phi_i dV = - \int_{\sigma_n} J_i^{\rightarrow}(\sigma) d\sigma^{\rightarrow} \quad (2.13)$$

$$(i=1,2; n=1,\dots,N)$$

Making the assumption for the corresponding nodal representation

$$-\frac{1}{V_n} \sum_{m=1}^M J_{inm} \sigma_{nm} \cong -w_{in} \phi_{in} + \sum_{m=1}^M (w_{inm} \phi_{in_m}) \quad (2.14)$$

$$(i=1,2; n=1,\dots,N)$$

means the diffusion term is expressed as a combination of neutron fluxes in node n and in its M_n neighbouring nodes n_m , introducing diagonal and non-diagonal spatial coupling coefficients (w_{in}, w_{inm}).

Thus, the diffusion eqs. (2.1) and (2.2) take the following algebraic form

$$-w_{1n} \phi_{1n} + \sum_{m=1}^M (w_{1nm} \phi_{1n_m}) - (\Sigma_{a1n} + \Sigma_{12n}) \phi_{1n} + \frac{U}{k} (\Sigma_{f1n} \phi_{1n} + \Sigma_{f2n} \phi_{2n}) = 0 \quad (2.15)$$

$$-w_{2n} \phi_{2n} + \sum_{m=1}^M (w_{2nm} \phi_{2n_m}) - \Sigma_{a2n} \phi_{2n} + \Sigma_{12n} \phi_{1n} = 0$$

$$(n=1,\dots,N) \quad (2.16)$$

The connection between the power density P_n and the corresponding fast and thermal neutron fluxes ϕ_{1n} and ϕ_{2n} at each node n is given by

$$P_n = E_{eff} (\Sigma_{f1n} \phi_{1n} + \Sigma_{f2n} \phi_{2n}) \quad (n=1,\dots,N) \quad (2.17)$$

If the net neutron current density values J_{inm} through the M_n surface parts σ_{nm} of the node n could be represented in a first approximation by the relation

$$J_{inm} = d_{inm}(\phi_{in} - \phi_{inm}) \quad (i=1,2; n=1,\dots,N; m=1,\dots,M_n) \quad (2.18)$$

it follows from the definition eq. (2.14) that the coupling coefficients could then be ascertained from the equations

$$w_{in} = \frac{1}{V_n} \sum_{m=1}^{M_n^R} (d_{inm} \sigma_{nm}) \quad (2.19)$$

$$w_{inm} = \frac{1}{V} d_{inm} \sigma_{nm} \quad (i=1,2; n=1,\dots,N; m=1,\dots,M_n) \quad (2.20)$$

(M_n^R = directions to reflector nodes included)

The method to establish the coefficients d_{inm} (and thus also the coupling coefficients w_{in} , w_{inm}) varies according to the position of the node within the total core partition.

- For nodes on the edge of the core pattern the coefficients d_{inm} can be determined at once by taking advantage of the characteristic feedback properties of the reflector or the given symmetry situation.
- To determine the coefficients d_{inm} (and thus also the spatial coupling coefficients) for the inner nodes of the core pattern, four principal approaches are possible:
 - coupling coefficients determined from analytical considerations,
 - coupling coefficients determined from measurements,
 - coupling coefficients determined only from basic model results,
 - coupling coefficients determined from basic model results and analytical considerations.

At present the last method is applied to establish GARLIC. This is done in two steps:

- Assuming in the first step in a very simple way an equivalent polygonal instead of a polynomial flux approximation (with conservation of the nodal values), the neutron flux gradient at a node boundary is then proportional to the difference in the mean neutron flux values of the corresponding neighbouring nodes, as required in eq. (2.18). Thus, starting from Fick's law the corresponding coefficients d_{inm} can be established by applying the usual finite-difference scheme

$$d_{inm} \cong 2 \sigma_{nm} / [V_n / D_{in} + V_m / D_{im}]$$

(i=1,2; n=1,...,N; 1,...,M_n) (2.21)

The nondiagonal spatial coupling coefficients w_{inm} can now be determined from eq. (2.20).

- Since the flux values are given from the calculations with the basic model the readjusted diffusion eqs. (2.15) and (2.16) have to stay valid. Thus, in a second step the diagonal coupling coefficients w_{in} are then also defined by these equations, taking into account these calculated flux values from the basic code.

2.5 1^{1/2} Group Representation

Considering eq. (2.16) for the thermal neutron energy group an approximate relation between the fast and the thermal neutron flux (called "spectrum index") can be derived

$$\phi_{2n} / \phi_{1n} = \Sigma_{12n} / [(1 - C_{L2n}) \Sigma_{a2n}] \cong (1 + C_{L2n}) \Sigma_{12n} / \Sigma_{a2n}$$

(n=1,...,N) (2.22)

by defining a "thermal leakage term"

$$\Sigma_{L2n} = -\omega_{2n} + \sum_{m=1}^{M_n} (\omega_{2inm} \phi_{2n_m} / \phi_{2n}) = \Sigma_{a2n} - \Sigma_{12n} \phi_{1n} / \phi_{2n}$$

(n=1, ..., N) (2.23)

and taking into account that Σ_{L2n} is small compared to 1 (lying in the range of $\pm 3\%$).

Replacing in the eq. (2.15) the neutron fluxes with the corresponding power density values using the relations

$$\phi_{1n} = (\epsilon_n - 1) P_n / (\epsilon_n E_{eff} \Sigma_{f1n}) \quad (2.24)$$

$$\phi_{2n} = P_n / (\epsilon_n E_{eff} \Sigma_{f2n}) \quad (n=1, \dots, N) \quad (2.25)$$

which follow from the eqs. (2.17) and (2.22) by introducing the "fast fission factor"

$$\epsilon_n = 1 + \Sigma_{a2n} \Sigma_{f1n} / (\Sigma_{12n} \Sigma_{f2n}) \quad (n=1, \dots, N) \quad (2.26)$$

and combining the original fast and thermal coupling coefficients into a new set of modified coupling coefficients of the form

$$\omega_n = \omega_{1n} + \omega_{2n} \cup \Sigma_{f2n} \Sigma_{12n} / (k \Sigma_{a2n}^2) \quad (2.27)$$

$$\omega_{nm} = \omega_{1nm} + \cup \Sigma_{f2n} \Sigma_{12n} \phi_{1n} \phi_{2nm} / (k \phi_{2n} \phi_{1nm} \Sigma_{a2n}^2)$$

(n=1, ..., N; m=1, ..., M_n) (2.28)

helps finally to reduce the two group representation to a "1 1/2 group formalism", yielding the following relation for the power density distribution

$$\sum_{j=1}^N [(F_{PW})_{nj} P_j] = \lambda P_n \quad (n=1, \dots, N) \quad (2.29)$$

The relation above represents a special eigenvalue problem with the state matrix

$$(F_{PW})_{nj} = (\lambda_n + w_n \eta_n) \delta_{nj} - \sum_{m=1}^M (w_{nm} \eta_n \delta_{nmj}) \quad (2.30)$$

$$(n=1, \dots, N; j=1, \dots, N; \delta_{nj} = \text{Kronecker symbol})$$

the eigenvector P_n , the eigenvalue $\lambda = 1/k - 1$ and the abbreviations

$$\eta_n = (\epsilon_n - 1) / (\epsilon_n v \Sigma_{f1n}) = 1 / (v \Sigma_{f1n} + v \Sigma_{f2n} \Sigma_{12n} / \Sigma_{a2n}) \quad (2.31)$$

$$\lambda_n = (\Sigma_{a1n} + \Sigma_{12n}) \eta_n^{-1} \quad (n=1, \dots, N) \quad (2.32)$$

2.6 Homogenization (Superbox Representation)

In order to get computer codes with a not too large demand in terms of computer storage and computer time, it is necessary to restrict the theoretical model to a minimum number of nodes, i.e., to represent the reactor by combining some basic volume elements to form superboxes (= nodes). Normally, these superboxes are assumed to be of a rectangular size. In order to be able to describe a jagged reactor core by a reasonable number of superboxes, however, superboxes in the vicinity of a reflector may be allowed to have a jagged shape.

The volume (V_n) of such a superbox (or node n) consists of h_n basic volume elements (V_h). Obviously, the characteristic parameters belonging to these basic volume (or coarse mesh) elements have to be generalized to the superbox (= nodal) representation too by applying suitable homogenizing (= rebalancing) procedures:

Xenon, iodine and power density and neutron flux values of a superbox n are determined by averaging the corresponding basic values weighted with the adequate volume elements. The homogenizing of the corresponding cross sections (and their derivatives) over a superbox is done by weighting them with volume times neutron flux values.

Special precautions had to be taken to describe the influence of a control rod movement on the macroscopic cross sections over a superbox (Ho, Lu 81).

Coupling coefficients have to be homogenized in such a way that the eigenvalue representation (2.29) for coarse mesh elements stays valid for the superbox concept too. Following a rebalancing method as proposed by SIEWERS (Si 76), such rebalanced coupling coefficients can be obtained according to the relations

$$\omega_n = \frac{1}{V_n P_n \eta_n} \sum_{h \in n} V_h \left\{ P_h [\eta_h \omega_h + \lambda_h - \lambda_n] + \sum_{k \in n} P_k \eta_k \omega_{hk} \sum_{m=1}^{M_n} \delta_{kh_m} \right\} \quad (2.33)$$

$$\omega_{nm} = \frac{1}{V_n P_n \eta_n} \sum_{h \in n} V_h \sum_{k \in n_m} (V_k P_k \eta_k \omega_{hk} \delta_{h_m k}) \quad (n=1, \dots, N; m=1, \dots, M_n) \quad (2.34)$$

(h_m = neighbour of h in m direction)

If starting with results obtained from calculations with a basic model, the elementary and thus, after homogenization, also the nodal power density values at the working point t_w are available.

If only the group constants and the spatial coupling coefficients are given by the basic model, the corresponding power

density distribution P_{nw} and the multiplication factor k have to be determined by solving the special eigenvalue problem as presented above.

A perturbation of the system affects the macroscopic cross sections and thus the power density distribution. To get a critical reactor, the multiplication factor k has to be equal to 1 and thus the eigenvalue λ equal to 0.

As can be seen from eq. (2.21) the coarse mesh coupling coefficients are mainly dependent on the distance between the centre points of the coarse mesh elements and their diffusion constants. Since the diffusion constants are not very sensitive against changes in the operation conditions, it can be expected that the corresponding coupling coefficients and - according to the eqs. (2.27) and (2.28) - also the modified ones will not vary much during one transient run. So, from eqs. (2.33) and (2.34) it follows that after rebalancing the coupling coefficients they can still be expected to stay almost constant for different operation conditions, i.e., $\omega_n \cong \omega_n$, $\omega_{nm} \cong \omega_{nm}$.

Starting from eq. (2.29) the transient behaviour of the power density, i.e., the pseudostationary relative variation $\delta_r P_n$ of the nodal power density around its working point values P_{nw} (with respect to a normalization value P_N) caused by inherent or outside perturbation of the system can now be described by the (non-linear) algebraic equation system

$$\sum_{j=1}^N [(F_{PW})_{njw} \delta_r P_j] = \delta_r L_n \quad (n=1, \dots, N) \quad (2.35)$$

with the time-dependent vector

$$\begin{aligned} \delta_r L_n = & -(P_n/P_N) [(\delta\Sigma_{an} + \delta\Sigma_{12n})\eta_n + (\Sigma_{anw} + \Sigma_{12nw} + \omega_{nw})\delta\eta_n] + \\ & + \sum_{m=1}^M [(P_n/P_N)\omega_{nmw} \delta\eta_m] \quad (n=1, \dots, N) \quad (2.36) \end{aligned}$$

and

$$\begin{aligned} \delta\eta_n = \eta_{nw} [& F_{xww}(n)\delta_r X_{e_n} + F_{fww}(n)\delta_r T_{Fn} + F_{cww}(n)\delta_r T_{Cn} + \\ & + F_{Aww}(n)\delta_r \alpha_n + \sum_{r=1}^R F_{uww}(n,r)\delta_r U_{nr}] \end{aligned} \quad (2.37)$$

$$\begin{aligned} \delta\Sigma_{a1n} = \Sigma_{a1}^X X_{e_n} \delta_r X_{e_n} + \Sigma_{a1}^F T_{Fn} \delta_r T_{Fn} + \Sigma_{a1}^C T_{Cn} \delta_r T_{Cn} + \\ + \Sigma_{a1}^D \rho_N^\alpha \delta_r \alpha_n + \frac{1}{\Delta z_n} \sum_{r=1}^R C_{1nr} \Delta\Sigma_{a1r} U_{Cn} \delta_r U_{nr} \end{aligned} \quad (2.38)$$

$$\begin{aligned} \delta\Sigma_{12n} = \Sigma_{12n}^X X_{e_n} \delta_r X_{e_n} + \Sigma_{12n}^F T_{Fn} \delta_r T_{Fn} + \Sigma_{12n}^C T_{Cn} \delta_r T_{Cn} + \\ + \Sigma_{12n}^D \rho_N^\alpha \delta_r \alpha_n + \frac{1}{\Delta z_n} \sum_{r=1}^R C_{1nr} \Delta\Sigma_{12r} U_{Cn} \delta_r U_{nr} \end{aligned} \quad (2.39)$$

with

$$\begin{aligned} F_{xww}(n) &= \left(\frac{X_{e_n}}{\eta_{nw}}\right) [D_{A2nw} \Sigma_{a2n}^X -D_{12nw} \Sigma_{12n}^X -D_{F1nw} \Sigma_{f1n}^X -D_{F2nw} \Sigma_{f2n}^X] \\ F_{fww}(n) &= \left(\frac{T_{Fn}}{\eta_{nw}}\right) [D_{A2nw} \Sigma_{a2n}^F -D_{12nw} \Sigma_{12n}^F -D_{F1nw} \Sigma_{f1n}^F -D_{F2nw} \Sigma_{f2n}^F] \\ F_{cww}(n) &= \left(\frac{T_{Cn}}{\eta_{nw}}\right) [D_{A2nw} \Sigma_{a2n}^C -D_{12nw} \Sigma_{12n}^C -D_{F1nw} \Sigma_{f1n}^C -D_{F2nw} \Sigma_{f2n}^C] \\ F_{Aww}(n) &= \left(\frac{\alpha_N \rho^\alpha}{\eta_{nw}}\right) [D_{A2nw} \Sigma_{a2n}^D -D_{12nw} \Sigma_{12n}^D -D_{F1nw} \Sigma_{f1n}^D -D_{F2nw} \Sigma_{f2n}^D] \\ F_{uww}(n) &= \left(\frac{U_{Nr}}{\eta_{nw}}\right) [D_{A2nw} \Sigma_{a2nw}^u -D_{12nw} \Sigma_{12nw}^u -D_{F1nw} \Sigma_{f1nr}^u -D_{F2nw} \Sigma_{f2nr}^u] \end{aligned} \quad (2.40)$$

3. THERMO- AND HYDRODYNAMIC CORE AND PLANT PARAMETERS

The important thermo-hydrodynamic parameters which describe the state of the reactor core and plant are coolant mass flow, steam quality, void fraction, coolant temperature, fuel rod temperature, system pressure, water level in top plenum, feed water mass flow, steam outlet flow, and the thermodynamic properties of the coolant fluid. For a precise calculation of the core power distribution and prediction of the local core and global plant states, these parameters must be calculated with sufficient accuracy under the constraints that are imposed by the plant control strategy.

3.1 Core Nodal Structure

The nodal structure that is used in GARLIC-B is such that nodes form nodal-columns in the vertical direction. The structure of a boiling water reactor allows no cross flows between the coolant channels of different fuel elements and as a result no cross flows occur between these nodal columns. The model assumes uniform velocity distribution within each nodal column even though they may contain more than one fuel element. Coolant water enters a nodal column at the bottom; it is heated up by the fuel rods as it flows up; starts boiling at a certain point and leaves the nodal column as a two-phase mixture of steam and water.

Numbering of the nodes is depicted in fig. 3.1. Index k indicates a specific nodal column, and the nodes that lie on it are numbered from bottom to top as

$$n = (k-1) n_z + 1, \dots, kn_z \quad (3.1)$$

where n_z is the total number of nodal layers within the core. The total number n_{xy} of nodal columns is given by

$$n_{xy} = \frac{N}{n_z} \quad (3.2)$$

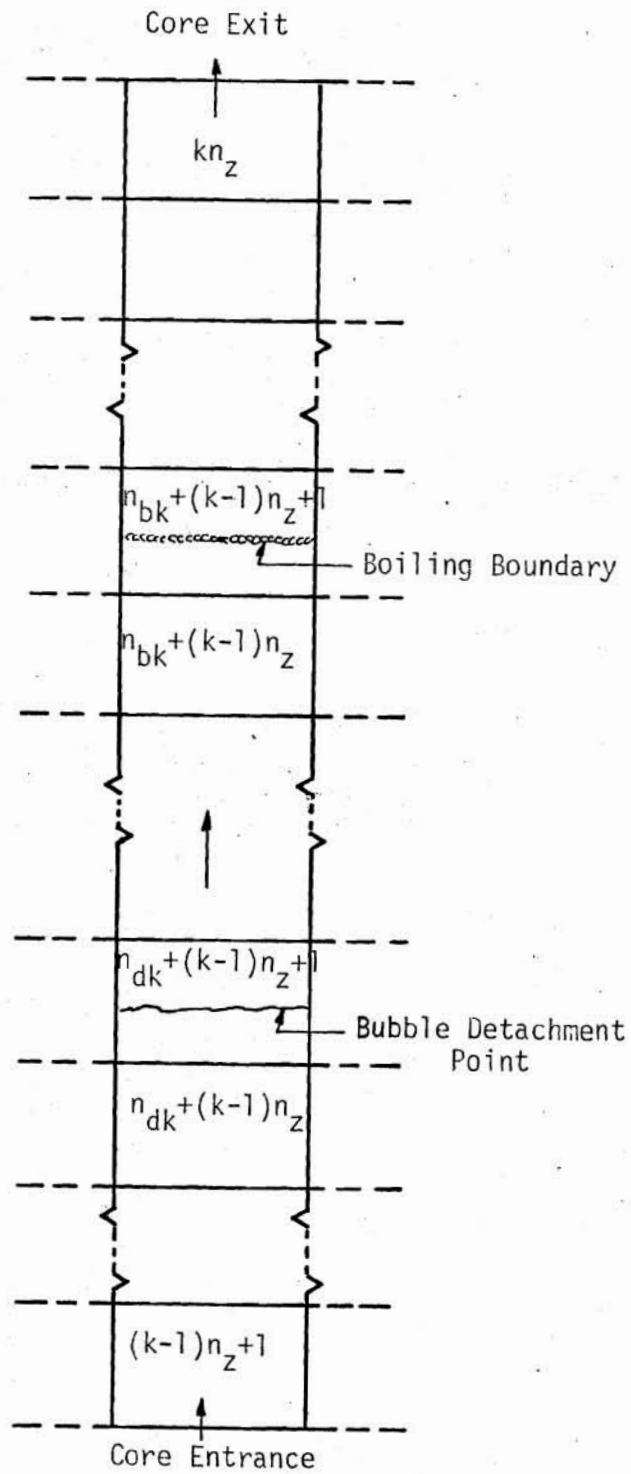


Figure 3.1:
Numbering Convention on a Nodal Column

As a result, all nodes within the core are numbered by shifting the index k in (3.1) as $k=1,2,\dots,n_{xy}$. The total number of nodes with one-phase flow in the k 'th nodal column is indicated by n_{dk} which will also be called the bubble detachment index of the k 'th nodal column. The indices of the nodes within which bubble detachment point¹⁾ lies, are then given by $n_{dk}+(k-1)n_z+1$ ($k=1,\dots,n_{xy}$). The total number of nodes with subcooled flow in the k 'th nodal column is named n_{bk} which is called also the boiling boundary index. Then, the indices of the nodes which carry boiling boundaries²⁾ are given by $n_{bk}+(k-1)n_z+1$ ($k=1,\dots,n_{xy}$).

3.2 Nodal Coolant Mass Flow Rate

Typical time step sizes that are used by GARLIC-B for transient calculations are sufficiently long (1-30 min.), such that steady state flow equations may be used. Hence, the coolant flow rate through a node may be taken the same as the flow rate G_{Ek} entering the nodal column on which it lies. So

$$G_n = G_{Ek} \quad (n=(k-1)n_z+1,\dots,kn_z \text{ and } k=1,\dots,n_{xy}) \quad (3.3)$$

is assumed both in static and transient calculations.

3.3 Steam Quality and Void Fraction

The model assumes that the fluid below the point of net vapor generation (also called the bubble detachment point) is entirely

¹⁾ Point of net vapor generation in subcooled boiling.

²⁾ Point where the bulk temperature of two phase water reaches the saturation temperature.

of onephase; hence, steam qualities and void fractions in this region are assumed to be zero.

Saha and Zuber (Sa,Zu 74) have derived the following correlation at the point of bubble detachment:

$$\begin{aligned} \text{Nu} &= \frac{q \cdot d_h}{k_f \cdot \Delta T_d} = 455 && \text{if } P_e \leq 70.000 \\ \text{St} &= \frac{q}{V \cdot h_w^T \Delta T_d} = 0.0065 && \text{if } P_e > 70.000 \end{aligned} \quad (3.4)$$

where q (J/m²-sec.) is the heat flux, V (kg/m²-sec.) is the fluid mass velocity, ΔT_d is the subcooling defined as

$$\Delta T_d = T_s - T_d \quad (3.5)$$

and Pe is the Peclet number which is defined as

$$Pe = \frac{\text{Nu}}{\text{St}} = \frac{V \cdot d_h \cdot h_w^T}{k_f} \quad (3.6)$$

The thermodynamic vapor quality at the point of bubble detachment can be written as

$$x_d = \frac{h_{dL} - h'}{h_{sw}} = - \frac{h_w^T \Delta T_d}{h_{sw}} \quad (3.7)$$

Then, substituting ΔT_d from (3.4) into (3.7) results in

$$x_d = -0.0022 \frac{q d_h h_w^T}{h_{sw} k_f} \quad \text{if } P_e \leq 70.000$$

$$x_d = -153.8 \frac{q}{V \cdot h_{sw}} \quad \text{if } Pe > 70.000 \quad (3.8)$$

3.3.1 Location of Bubble Detachment Point

In order to find the location of the bubble detachment point, bulk fluid temperatures at node exits (T_{ie}) and the corresponding subcoolings $T_s - T_{ie}$ are calculated starting from the node at the bottom of the channel. The bubble detachment point lies within the node at the exit of which $T_s - T_{ie}$ becomes less than ΔT_d .

Fluid temperatures at node exits are obtained from the following equations:

$$T_{cne} = T_{cni} + \frac{V_n P_n}{G_k h_w T} \quad (3.9a)$$

and

$$T_{cni} = T_E \quad \text{for } n = (k-1) n_z + 1 \quad (k=1, \dots, n_{xy}) \quad (3.9b)$$

Then, location of the bubble detachment point within the node is obtained from

$$\Delta z_{dk} = \frac{\Delta z_n G_k h_w T}{V_n P_n} (T_s - T_{cni} - \Delta T_d) \quad (3.10)$$

where Δz_{dk} is the distance of the bubble detachment point to the node entrance.

When power density distribution increases drastically from one node to its downstream neighbor, difficulties may arise in determining the location of the bubble detachment point. The problem is depicted in fig. 3.2.

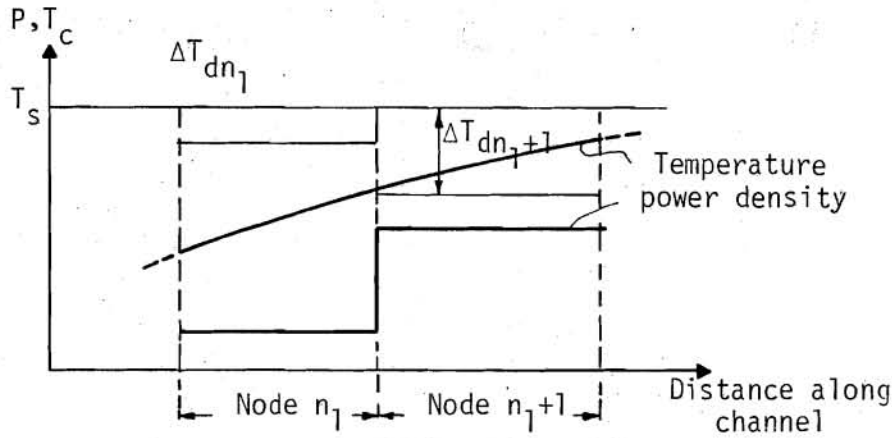


Figure 3.2:
Depiction of the Need for a Border Zone

In the figure, the heat flux in node- n_1 is sufficiently low so that the water temperature has not reached $T_s - \Delta T_{dn}$, at the node exit. In the n_1+1 'th node, power density, and as a result, the heat flux and $\Delta T_{d,n_1+1}$ are much higher. The value of $\Delta T_{d,n_1+1}$ is so large that $T_s - \Delta T_{d,n_1+1}$ is lower than the water temperature at the node entrance. Hence looking from node n_1 , the bubble detachment point should lie in node n_1+1 ; whereas, looking from node n_1+1 , it should lie in node n_1 .

In such cases, more refined calculations are carried out while passing from one node to the next. The approach is approximate, however, should be better than taking the bubble detachment point at the entrance of node n_1+1 , in which the water temperature becomes higher than $T_s - \Delta T_{di}$ for the first time.

The method assumes a linearly increasing power density distribution within a border zone which extends from both sides of the common node boundary to equal distances up to the mid-point of the shorter of the two nodes. Power density distribution is depicted in fig. 3.3.

Obviously, assumptions concerning the width of the border zone and the shape of the power density distribution in it may be in considerable error. However, assuming and using nodal power

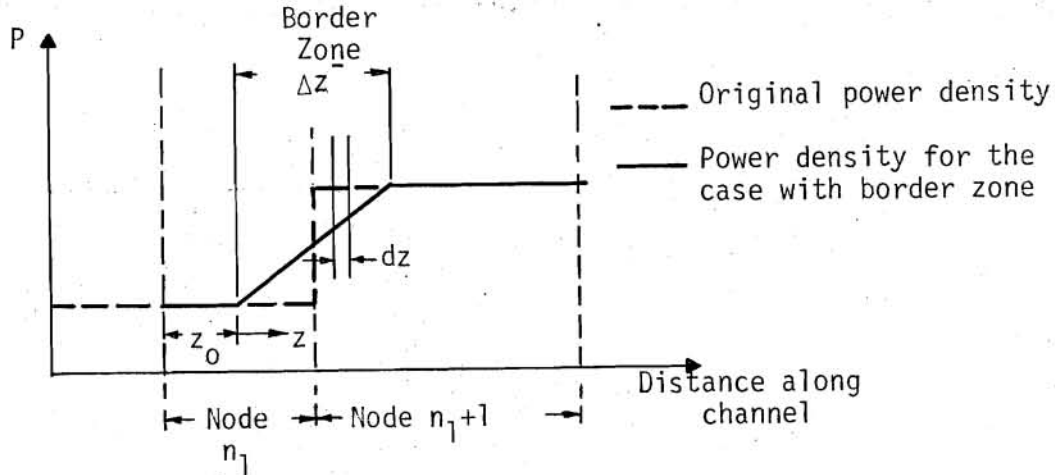


Figure 3.3:
Construction of a Border Zone

density values in GARLIC-B calculations rather than the actual distributed values are more radical than the above assumption. The above assumption in fact replaces the nodal power density distribution by a distribution that is closer to reality.

For the linear power density distribution the distance of the bubble detachment point z_{xk} to the border zone entrance is found as the smaller positive root of the following quadratic equation:

$$\begin{aligned}
 & \frac{A_{tk}(P_{n_1+1}-P_{n_1})}{2h_w^T G_k \Delta z^-} z_{xk}^2 \left[\frac{(P_{n_1+1}-P_{n_1})d_h}{455 k_f S_f A_r \Delta z^-} + \frac{A_{tk} P_{n_1}}{h_w^T G_k} \right] z_{xk} + \\
 & + T_{Bzi} - T_s + \frac{P_{n_1} d_h}{455 k_f S_f A_r} = 0 \quad \text{if } Pe \leq 70.000
 \end{aligned} \tag{3.11}$$

$$\begin{aligned}
 & \frac{A_{tk}(P_{n_1+1}-P_{n_1})}{2h_w^T G_k \Delta z^-} z_{xk}^2 + \left[\frac{(P_{n_1+1}-P_{n_1})}{0.0065 S_f A_r V h_w^T \Delta z^-} + \frac{A_{tk} P_{n_1}}{h_w^T G_k} \right] z_{xk} + \\
 & + T_{Bzi} - T_s + \frac{P_{n_1}}{0.0065 S_f A_r V h_w^T} = 0 \quad \text{if } Pe > 70.000
 \end{aligned}$$

where A_{tk} and A_k are the total area and the net flow area of the k 'th channel, S_f is the fuel periphery per unit flow area, and

$$A_r = \frac{A_k}{A_{tk}} = \dots = \frac{A_i}{A_{ti}} \quad (3.12)$$

is the area ratio,

$$\Delta z^- = \min (\Delta z_{n_1}, \Delta z_{n_1+1}) \quad (3.13)$$

is the width of the border zone, and ΔT_{Bzi} is the water temperature at the border zone entrance given by

$$T_{Bzi} = T_{cni} + \frac{V_{n_1} P_{n_1} (\Delta z_{n_1} - \frac{\Delta z^-}{2})}{G_k h_w^T \Delta z_{n_1}} \quad (3.14)$$

3.3.2 Steam Quality and Void Fraction Distributions for the Transient Case

The thermodynamic quality x_{ne} at the exit of a node with uniform power distribution may be obtained as follows from the energy and mass balance equations, assuming that the void fraction dynamics are fast enough so that quasistatic equations may be used:

$$x_{ne} = x_{ni} + \frac{1}{h_{sw} G_k} (V_n P_n - D_{PN,n} \dot{p}) \quad (3.15)$$

with

$$D_{PN,n} = V_n \{ \rho' h'^P - 1 - (1 - \alpha_n) \rho' h_{sw} x_{ne} + \alpha_n [(1 - x_{ne}) \rho'' h_{sw} + \rho'' h''^P - \rho' h'^P] \} \rho' h'^P (1 - \alpha_n) \quad (3.16)$$

The last term in parenthesis of eq. (3.15) represents the condensation effect resulting from system pressure changes. Counterpart of eq. (3.15) for a cross-sectional element of length dz in node n is

$$dx = \frac{1}{h_{sw} G_k \Delta z_n} (V_n P_n - D_{PN,n} \dot{p}) dz \quad (3.17)$$

where the condensation effect is included only approximately since the nodal value of $D_{PN,n}$ (eq. 3.16) is used rather than the local value. For the cases where the nodal power distribution is not uniform (such as in border zones) P_n in eq. (3.17) is replaced by the local value $P(z)$.

Model assumes that true quality is related to the thermodynamic quality through the following empirical relationship (Bu,He 77):

$$x_t = x - x_d \exp\left(\frac{x}{x_d} - 1\right) \quad (3.18)$$

Void fractions are calculated from the Bankoff (Ba 60) two phase correlation which assumes a slip ratio of the form

$$S = \frac{1-\alpha}{K_B^{-\alpha}} \quad (3.19)$$

and is expressed as

$$\alpha = K_B \frac{\rho' x}{\rho' x + (1-x)\rho''} \quad (3.20)$$

with

$$K_B = 0.71 + 1.45 \times 10^{-8} p \quad (p \text{ in N/m}^2) \quad (3.21)$$

3.3.2.1 Case A: Channels without Border Zone

- Nodes with Point of Bubble Detachment

Thermodynamic quality distribution within the subcooled boiling part of the node is

$$x(z') = x_d + \frac{(V_n^P - D_{PN,n}\dot{p})}{h_{sw} G_k \Delta z_n} z' \quad (3.22)$$

where z' is measured from the bubble detachment point. Then, the value at the node exit is given by

$$x_e = x_d + \frac{(V_n^P - D_{PN,n}\dot{p})(\Delta z_n - \Delta z_{dk})}{h_{sw} G_k \Delta z_n} \quad (3.23)$$

The true quality distribution becomes

$$x_t(z') = x_d + \xi_n z' - x_d \exp \frac{\xi_n z'}{x_d} \quad (3.24)$$

with

$$\xi_n = \frac{V_n^P - D_{PN,n}\dot{p}}{h_{sw} G_k \Delta z_n} \quad (3.25)$$

Assuming that \dot{p} is independent of space, one obtains the following equation for the average true quality within the subcooled part of the node:

$$x_{tBM} = \frac{x_d + x_e}{2} - \frac{x_d^2}{x_e - x_d} [e^{(x_e - x_d)/x_d} - 1] \quad (3.26)$$

Then, the nodal average true quality is obtained as

$$x_{tn} = \left(1 - \frac{\Delta z_{dk}}{\Delta z_n}\right) x_{tBM} \quad (3.27)$$

Void fraction in the boiling part of the node α_{BM} and the average nodal void fraction α_n become

$$\alpha_{BM} = B(x_{tBM}, p) \quad (3.28)$$

$$\alpha_n = \left(1 - \frac{\Delta z_{dk}}{\Delta z_n}\right) \alpha_{BM} \quad (3.29)$$

where $B(x, p)$ is the Bankoff two phase correlation.

● Boiling Nodes without Point of Bubble Detachment

Distribution of true quality within the node is given by

$$x_t(z) = x_{ni} + \frac{(V_n P_n - D_{PN, n\dot{p}})}{h_{sw} G_k \Delta z_n} z - x_d \exp\left(\frac{x_{ni}}{x_d} + \frac{(V_n P_n - D_{PN, n\dot{p}})}{h_{sw} G_k x_d \Delta z_n} z - 1\right) \quad (3.30)$$

Then, the average nodal quality is obtained as

$$x_{tn} = x_{ni} + \frac{V_n P_n - D_{PN, n\dot{p}}}{2h_{sw} G_k} - \frac{h_{sw} G_k x_d^2}{V_n P_n - D_{PN, n\dot{p}}} \left[\exp\left(\frac{x_{ni}}{x_d} - 1\right)\right] \cdot \left[\exp\left(\frac{V_n P_n - D_{PN, n\dot{p}}}{h_{sw} G_k x_d}\right) - 1\right] \quad (3.31)$$

which leads to a nodal void fraction as

$$\alpha_n = B(x_{tn}, p) \quad (3.32)$$

3.3.2.2 Case B: Channels with Border Zone

- Nodes with Border Zone

Suppose that nodes n_1 and n_1+1 carry the border zone. These nodes require special attention since power density distribution within the border zone is nonuniform.

One of the following two cases is possible depending on the location of the bubble detachment point:

- (1) Bubble Detachment Point is in Node n_1 .

The case is shown in fig. 3.4.

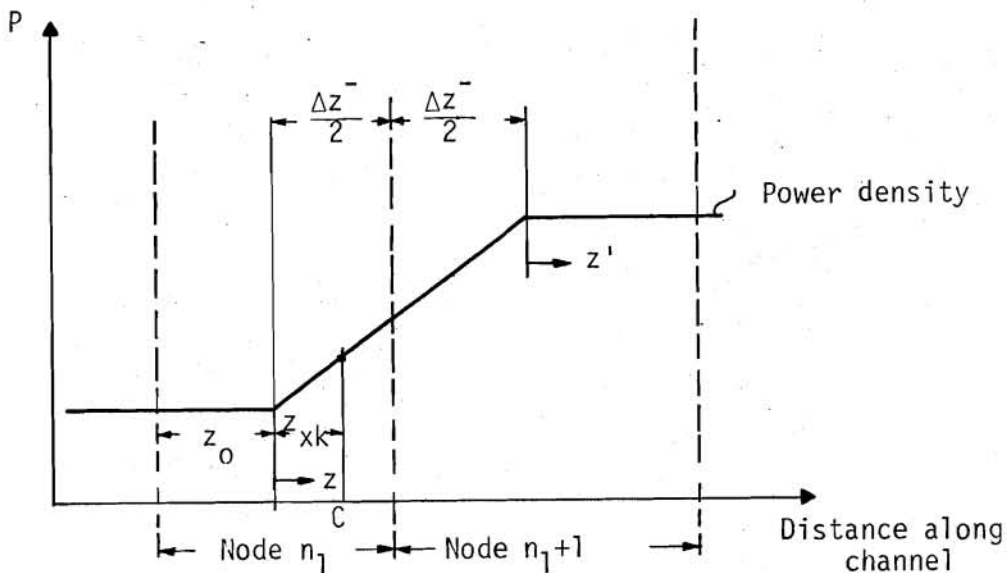


Figure 3.4:

Channel with Border Zone

Bubble Detachment Point (C) is in Node n_1

The thermodynamic quality distribution is found by substituting the linear power density distribution $P(z)$ into (3.17) integrating the latter from z_{xk} to z :

$$x(z) = \eta_0 + \eta_1 z^2 + \eta_2 z \quad (3.33)$$

with

$$\eta_2 = \frac{A_{tk} P_{n_1}}{h_{sw} G_k} - \frac{D_{PN, n_1} \dot{p}}{h_{sw} G_k \Delta z_{n_1}} \quad (3.34)$$

$$\eta_1 = \frac{A_{tk} (P_{n_1+1} - P_{n_1})}{2h_{sw} G_k \Delta z^-} \quad (3.35)$$

$$\eta_0 = x_d - \eta_1 z_{xk}^2 - \eta_2 z_{xk} \quad (3.36)$$

Then, the true quality distribution is

$$x_t(z) = \eta_0 + \eta_1 z^2 + \eta_2 z - x_d \exp[(\eta_1/x_d)(z^2 - z_{xk}^2) + (\eta_2/x_d)(z - z_{xk})] \quad (3.37)$$

Integrating the true quality distribution within the subcooled boiling part yields the average true quality as

$$\begin{aligned} x_{tBM} = & \frac{1}{\frac{\Delta z^-}{2} - z_{xk}} \left\{ \eta_0 \left(\frac{\Delta z^-}{2} - z_{xk} \right) + \frac{\eta_1}{3} \left[\left(\frac{\Delta z^-}{2} \right)^3 - z_{xk}^3 \right] + \frac{\eta_2}{2} \left[\left(\frac{\Delta z^-}{2} \right)^2 - z_{xk}^2 \right] - \right. \\ & \left. - x_d \left[\exp\left(-\frac{\eta_1}{x_d} z_{xk}^2 - \frac{\eta_2}{x_d} z_{xk}\right) \right] I_{zn_1} \right\} \quad (3.38) \end{aligned}$$

with

$$I_{zn_1} = \int_{z_{xk}}^{\frac{\Delta z^-}{2}} \exp\left(\frac{\eta_1}{x_d} z^2 + \frac{\eta_2}{x_d} z\right) dz \quad (3.39)$$

which is evaluated numerically.

The nodal true quality is

$$x_{tn_1} = \left(\frac{\frac{\Delta z^-}{2} - z_{xk}}{\Delta z_{n_1}^-} \right) x_{tBM} \quad (3.40)$$

Then,

$$\alpha_{BM} = B(x_{tBM}, p) \quad (3.41)$$

and

$$\alpha_{n_1} = \left(\frac{\frac{\Delta z^-}{2} - z_{xk}}{\Delta z_{n_1}^-} \right) \alpha_{BM} \quad (3.42)$$

The average true quality within the border zone of node n_1+1 can be obtained in a similar manner by integrating eq. (3.37):

$$x_{tBz} = \frac{2}{\Delta z^-} \left\{ \eta_0 \left(\frac{\Delta z^-}{2} \right) + \frac{\eta_1}{3} [(\Delta z^-)^3 - \left(\frac{\Delta z^-}{2} \right)^3] + \frac{\eta_2}{2} [(\Delta z^-)^2 - \left(\frac{\Delta z^-}{2} \right)^2] - \right. \quad (3.43)$$

$$\left. -x_d \left[\exp\left(-\frac{\eta_1}{x_d} z_{xk}^2 - \frac{\eta_2}{x_d} z_{xk}\right) \right] I_{z, n_1+1} \right\}$$

with

$$I_{z, n_1+1} = \int_{\frac{\Delta z^-}{2}}^{\Delta z^-} \exp\left(\frac{\eta_1}{x_d} z^2 + \frac{\eta_2}{x_d} z\right) dz \quad (3.44)$$

which is evaluated numerically.

The thermodynamic quality at the exit of border zone is

$$x_{Bze} = \eta_0 + \eta_1 (\Delta z^-)^2 + \eta_2 \Delta z^- \quad (3.45)$$

The thermodynamic quality in the part that lies outside of border zone is

$$x(z') = x_{Bze} + \xi z' \quad (3.46)$$

where

$$\xi = \frac{A_{tk}^P n_{1+1}}{h_{sw} G_k} - \frac{D_{PN, n_{1+1}} \dot{p}}{h_{sw} G_k \Delta z_{n_{1+1}}} \quad (3.47)$$

and z' is measured from the exit of border zone. The true quality in this region is given by

$$x_t(z') = x_{Bze} + \xi z' - x_d \exp\left(\frac{x_{Bze}}{x_d} + \frac{\xi}{x_d} z' - 1\right) \quad (3.48)$$

The average true quality in this part of the node becomes

$$x_{tNBz} = \frac{1}{(\Delta z_{n_{1+1}} - \frac{\Delta z^-}{2})} \left\{ x_{Bze} (\Delta z_{n_{1+1}} - \frac{\Delta z^-}{2}) + \frac{\xi (\Delta z_{n_{1+1}} - \frac{\Delta z^-}{2})^2}{2} - x_d \exp\left(\frac{x_{Bze}}{x_d} - 1\right) \frac{x_d}{\xi} \left[\exp\left[\frac{\xi}{x_d} (\Delta z_{n_{1+1}} - \frac{\Delta z^-}{2})\right] - 1 \right] \right\} \quad (3.49)$$

Then, the average nodal true quality is

$$x_{tn_{1+1}} = \left[x_{tBz} \frac{\Delta z^-}{2} + x_{tNBz} (\Delta z_{n_{1+1}} - \frac{\Delta z^-}{2}) \right] \frac{1}{\Delta z_{n_{1+1}}} \quad (3.50)$$

and

$$\alpha_{n_{1+1}} = B(x_{tn_{1+1}}, P) \quad (3.51)$$

(2) Bubble Detachment Point is in node n_1+1 .

The case is depicted in fig. 3.5.

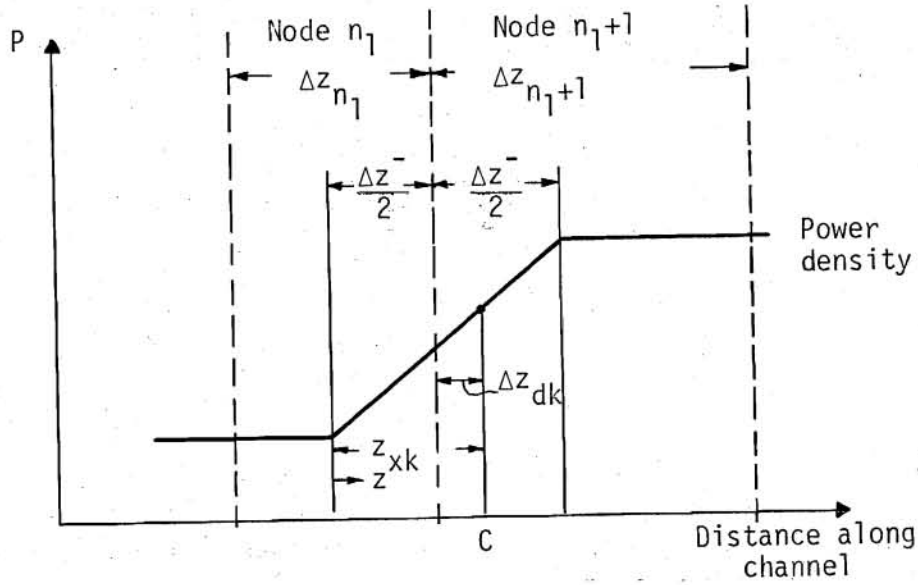


Figure 3.5:

Channel with Border Zone.

Bubble Detachment Point (C) in Node n_1+1

The thermodynamic quality distribution in border zone of node n_1+1 is

$$x(z) = x_d + \eta_1(z^2 - z_{xk}^2) + \eta_2(z - z_x) = \eta_0 + \eta_1 z^2 + \eta_2 z \quad (3.52)$$

where η_0 , η_1 and η_2 are defined by eqs. (3.34-3.36) with D_{PN, n_1} and Δz_{n_1} in (3.35) substituted by D_{PN, n_1+1} and Δz_{n_1+1} respectively.

The thermodynamic quality at border zone exit is

$$x_{Bze} = \eta_0 + \eta_1(\Delta z^-)^2 + \eta_2(\Delta z^-) \quad (3.53)$$

The true quality distribution in the border zone is the same as in eq. (3.37). The average true quality within the boiling part of border zone is

$$x_{tBz} = \frac{1}{\Delta z^- - z_{xk}} \left\{ \eta_0 (\Delta z^- - z_{xk}) + \frac{\eta_1}{3} [(\Delta z^-)^3 - z_{xk}^3] + \frac{\eta_2}{2} [(\Delta z^-)^2 - z_{xk}^2] - x_d \left[\exp\left(-\frac{\eta_1}{x_d} z_{xk}^2 - \frac{\eta_2}{x_d} z_{xk}\right) \right] I'_z \right\} \quad (3.54)$$

where

$$I'_z = \int_{z_x}^{\Delta z^-} \exp\left(\frac{\eta_1}{x_d} z^2 + \frac{\eta_2}{x_d} z\right) dz \quad (3.55)$$

which is evaluated numerically.

Thermodynamic and true qualities outside of the border zone are given by (3.46-3.47) and (3.48) with x_{Bze} given by eq. (3.53). The average true quality in the region outside of the border zone is given by eq. (3.49). The average true quality and void fraction in the boiling part of the node are given by

$$x_{tBM} = \left\{ x_{tBz} (\Delta z^- - z_{xk}) + x_{tNBz} \left(\Delta z_{n_1+1} - \frac{\Delta z^-}{2} \right) \right\} \frac{1}{(\Delta z_{n_1+1} - \Delta z_{dk})} \quad (3.56)$$

$$\alpha_{BMk} = B(x_{tBM}, p) \quad (3.57)$$

The average nodal true quality and void fraction are

$$x_{tn_1+1} = \left\{ x_{tBz} (\Delta z^- - z_{xk}) + x_{tNBz} \left(\Delta z_{n_1+1} - \frac{\Delta z^-}{2} \right) \right\} \frac{1}{\Delta z_{n_1+1}} \quad (3.58)$$

$$\alpha_{n_1+1} = \alpha_{\text{BMk}} \frac{\Delta z_{n_1+1}^{-\Delta z_{dk}}}{\Delta z_{n_1+1}} \quad (3.59)$$

● Nodes without Border Zone

Eqs. (3.30) and (3.32) are valid for nodes which lie downstream of node n_1+1 .

3.3.3 Steam Quality and Void Fraction Distribution at Working Point

At the working point \dot{p} is equal to zero; hence, equations (3.15) and (3.17) become respectively

$$x_{ne} = x_{ni} + (V_n P_n) / (G_k h_{sw}) \quad (3.60)$$

and

$$dx = \frac{V_n P_n}{G_k h_{sw} \Delta z_n} dz = \frac{A_{tk} P_n}{G_k h_{sw}} dz \quad (3.61)$$

where P_n in (3.61) is to be replaced by $P(z)$ if the element is in a border zone.

The equations are obtained from those for transient calculations by substituting $\dot{p} = 0$.

3.4 Coolant Mass Flow Distribution

Under quasi-static conditions, the total pressure drop along the k 'th nodal column is given by

$$\Delta p_k = \Delta p_{sk} + \Delta p_{Fk} + \Delta p_{Ak} + \Delta p_{Ik} \quad (k=1, \dots, n_{xy}) \quad (3.62)$$

where Δp_{sk} , Δp_{Fk} and Δp_{Ak} represent the pressure drops due to static head difference, friction and fluid acceleration respectively. The term Δp_{Ik} represents mainly the pressure drop due to inlet throttling; however, effects of spacers, elbows, etc. may also be included in this term depending on the structure of the reactor core.

For the present case, the total static pressure drop is

$$\Delta p_{sk} = \frac{1}{2} g z_{dk} (\rho_{wE} + \rho') + \sum_{n=(k-1)n_z + n_{dk} + 2}^{kn_z} g \Delta z_n [(1 - \alpha_n) \rho' + \alpha_n \rho''] + g (\Delta z_{n_{dk}+1} - \Delta z_{dk}) [(1 - \alpha_{BM,k}) \rho' + \alpha_{BM,k} \rho''] \quad (3.63)$$

where the three main terms represent respectively the static pressure drops due to i) non-boiling region of the nodal column, ii) nodes with two phase flow and iii) two-phase part of the node with the bubble detachment point, $\alpha_{BM,k}$ is the mean void fraction within the boiling part of the node with the bubble detachment point.

Friction pressure drop is obtained by summing the contributions of the boiling and non-boiling regions and is expressed as

$$\Delta p_{Fk} = \frac{z_{dk} \lambda_{NFR} G_k^2}{4 d_{Hk} A_k^2} \left(\frac{1}{\rho'} + \frac{1}{\rho_{wE}} \right) + \frac{\lambda_{BFR} G_k^2 z_H}{2 d_{Hk} \rho' A_k^2 z_{dk}} \int \phi[x(z), p(z)] dz \quad (3.64)$$

where λ_{NFR} and λ_{BFR} are the Darcy-Weisbach friction factors for non-boiling and boiling regions respectively and obtained from a correlation given by Moody (Mo 48). ϕ_n is the nodal Martinelli-Nelson two-phase friction pressure gradient multiplier (Ma, Ne 48) defined as

$$\phi_n(x_n, p) = \exp\{f_1 x_n / \sqrt{1 + f_2 x_n + f_3 x_n^2}\} \quad (3.65)$$

with

$$\begin{aligned} f_1 &= 44.216 + 7.4282 \times 10^{-7} p \\ f_2 &= 12.645 + 4.9841 \times 10^{-6} p \\ f_3 &= 17.975 + 2.5744 \times 10^{-5} p \end{aligned} \quad (p \text{ in N/m}^2)$$

and

$$\phi_{BM,k} = \phi_n(x_{BM,k}, p)$$

The pressure drop due to acceleration of fluid consists also of components contributed by the non-boiling and boiling regions, and is given by

$$\Delta p_{Ak} = \frac{G_k^2}{A_k^2} \left(\frac{1}{\rho'} - \frac{1}{\rho_{wE}} \right) + \frac{G_k^2}{A_k^2 \rho'} \left[\frac{(1-x_{knz,e})^2}{(1-\alpha_{knz,e})} \left(1 + \frac{x_{knz,e}}{1-x_{knz,e}} S_{knz,e} \right) - 1 \right] \quad (3.66)$$

where $\alpha_{knz,e}$, $x_{knz,e}$ and $S_{knz,e}$ represent the void fraction, steam quality and slip coefficient at the exit of node $n=kn_z$.

The pressure drop inlet throttling may be expressed as

$$\Delta p_{Ik} = r_k G_k^2 \quad (3.67)$$

where r_k is the channel inlet resistance defined as

$$r_k = \frac{1}{2\rho C_d^2 A_{ko}^2} \quad (3.68)$$

where A_{ko} is the orifice area at the channel inlet.

Substituting eqs. (3.63, 3.64, 3.66, 3.68) into (3.61) and rearranging the terms result in

$$\Delta p_k = \psi_k + \gamma_k G_k^2 \quad (3.69)$$

where

$$\begin{aligned} \psi_k = & \frac{1}{2} g z_{dk} (\rho_{wE} + \rho') + \sum_{n=(k-1)n_z + n_{dk} + 2}^{kn_z} g \Delta z_n [(1-\alpha_n)\rho' + \alpha_n \rho''] + \\ & + g (\Delta z_{n_{bk} + 1} - \Delta z_{dk}) [(1-\alpha_{BM,k})\rho' + \alpha_{BM,k} \rho''] \end{aligned} \quad (3.70)$$

and

$$\begin{aligned} \gamma_k = & \frac{z_{dk} \lambda_{NFR}}{4 d_{HK} A_k^2} \left(\frac{1}{\rho'} + \frac{1}{\rho_{wE}} \right) + \frac{1}{A_k^2} \left(\frac{1}{\rho'} - \frac{1}{\rho_{wE}} \right) + \\ & + \frac{\lambda_{BFR}}{2 d_{HK} \rho' A_k^2} [\phi_{BM,k} (\Delta z_{n_{dk} + 1} - \Delta z_{Bk}) + \sum_{n=(k-1)n_z + n_{dk} + 2}^{kn_z} \phi_n \Delta z_n] + \\ & + \frac{1}{A_k^2 \rho'} \left[\frac{(1-x_{kn_z,e})^2}{(1-\alpha_{kn_z,e})} \left(1 + \frac{x_{kn_z,e}}{1-x_{kn_z,e}} S_{kn_z,e} \right) - 1 \right] + r_k \end{aligned} \quad (3.71)$$

Since the pressure drops Δp_k along the nodal columns are equal to each other, one can write an equation similar eq. (3.69) for each one of the nodal columns and equate them to each other in order to find a relationship between the flows of different channels. For example, i'th and j'th columns yield

$$G_j = \left[\frac{\psi_k - \psi_j}{\gamma_j} + G_k^2 \frac{\gamma_k}{\gamma_j} \right]^{1/2} \quad (3.72)$$

On the other hand, the sum of all channel flows is equal to the total core flow; hence,

$$G_E = \sum_{j=1}^{n_{xy}} \left[\frac{\psi_k - \psi_j}{\gamma_j} + G_k^2 \frac{\gamma_k}{\gamma_j} \right]^{1/2} \quad (3.73)$$

Eq. (3.73) relates the flow through the k'th column to the total flow G_E .

Another useful expression is obtained by writing G_k as a function of the total pressure drop between core inlet and outlet. If Δp_z denotes this pressure drop ($\Delta p_z = \Delta p_k$, $k = 1, \dots, n_{xy}$), then

$$G_k = \left[\frac{\Delta p_z - \psi_k}{\gamma_k} \right]^{1/2} \quad (3.74)$$

The above presented quasistatic analysis for coolant flow distribution is used in the model also for the transient calculations.

3.5 Nodal Coolant Temperature Distribution

3.5.1 Transient Calculations

3.5.1.1 Channels without Border Zone

● Nodes with Single-Phase Flow

These are the nodes which are before the point of bubble detachment. The coolant temperatures of these nodes are calculated from the following equations.

$$T_{cne} = T_{cni} + (V_n P_n) / (G_k h_w^T) \quad (3.75)$$

$$T_{cni} = T_E \quad \text{if } n=(k-1)n_z+1 \quad (k=1, \dots, n_{xy}) \quad (3.76)$$

$$T_{cn} = \frac{1}{2} (T_{cni} + T_{cne}) \quad (3.77)$$

● Nodes with Subcooled Boiling

The energy equation for the two-phase region of the node becomes as follows by assuming that void fraction dynamics are sufficiently fast so that $\dot{\alpha}$ -terms may be dropped out, and that the steam phase has the enthalpy and temperature of saturated vapor at all times:

$$\begin{aligned} & (A_k/G_k) [\rho''h''^P + h''\rho''^P + (1-\alpha) \rho_w^P h_w + (1-\alpha) \rho_w h_w^P - 1] \dot{p} + \\ & + (h'' - h_w) (dx_t/dz) + [x_t h''^P + (1-x_t) h_w^P] (dp/dz) + \\ & + (1-x_t) h_w^T (dT_w/dz) = q/G_k \end{aligned} \quad (3.78)$$

But,

$$h_w = h' - h_w^T [T_s - T_w(z)] \quad (3.79)$$

Substitution of h_w from (3.79) into (3.78), then multiplying both sides of (3.78) by dz and rearranging its terms yield

$$\begin{aligned} dT_w = & \frac{1}{(1-x_t)h_w^T} \left\{ \frac{q}{G_k} - \frac{A_k}{G_k} [\rho''h''^P + h''\rho''^P + (1-\alpha) \rho_w^P h_w + (1-\alpha) \rho_w h_w^P - 1] \dot{p} - \right. \\ & \left. - [h_{sw} + h_w^T (T_s - T_w(z))] \frac{dx_t}{dz} - [x_t h''^P + (1-x_t) h_w^P] \frac{dp}{dz} \right\} dz \end{aligned} \quad (3.80)$$

The term dx_t/dz in eq. (3.80) will be substituted from the empirical subcooled boiling correlation, \dot{p} is obtained as in eq. (3.120) of section 3.7, (dp/dz) is taken as constant for each node and calculated from the nodal pressures by interpolation as

$$p_{zn} = \frac{dp}{dz} = \frac{1}{2} \left[\frac{p_{cn+1} - p_{cn}}{0.5(\Delta z_{n+1} + \Delta z_n)} + \frac{p_{cn} - p_{cn-1}}{0.5(\Delta z_n + \Delta z_{n+1})} \right] \quad (3.81)$$

Integration of eq. (3.80) gives the liquid water temperature distribution in the two-phase flow regions of the channel. Once, the liquid water temperature is known, the bulk temperature of the two-phase mixture is obtained from

$$T_c(z) = T_w(z)[1-x_t(z)] + T_s x_t(z) \quad (3.82)$$

● Nodes which Carry the Point of Bubble Detachment

a) Case without Boiling Boundary

The case is depicted in fig. 3.6. The temperature is assumed to increase linearly from T_{ni} , which is obtained from (3.75), at point A, to $T_s - \Delta T_d$ at point C. The true quality distribution from C to E is given by eq. (3.24).

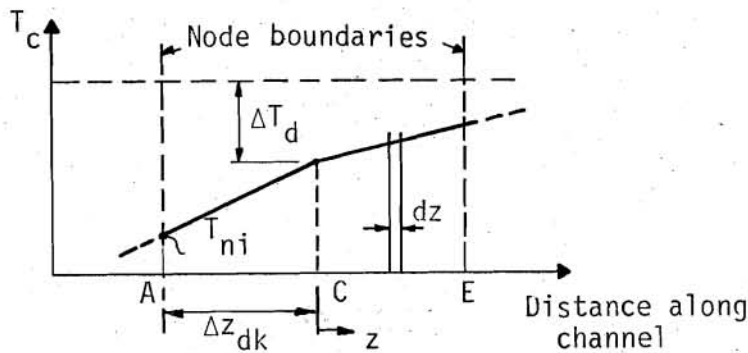


Figure 3.6:
Channel without Border Zone. Node with Bubble Detachment Point (C), without Boiling Boundary

Then,

$$dx_t/dz = \xi_n - \xi_n \exp[(\xi_n/x_d)z] \quad (3.83)$$

where ξ_n is defined as in eq. 3.25.

Substituting (3.81), (3.83) and $q = V_n P_n / \Delta z_n$ into (3.80) gives

$$dT_w = \frac{1}{h_w^T (1-x_d - \xi_n z/x_d e^{\xi_n z/x_d})} \left\{ \frac{V_n P_n}{G_k \Delta z_n} - \frac{A_k}{G_k} [\rho'' h''^P + h'' \rho''^P + (1-\alpha_n) (\rho_w^P h_w + \rho_w h_w^P) - 1] \dot{p} - [h_{sw} + h_w^T (T_s - T_w(z))] \xi_n (1 - e^{\xi_n z/x_d}) - [(h''^P - h_w^P) (x_d + \xi_n z - x_d e^{\xi_n z/x_d}) + h_w^P] p_{zn} \right\} dz \quad (3.84)$$

where

$$\rho_w = [(\rho' - \rho_{we})(T_w - T_e) / (T_s - T_e)] + \rho_{we}$$

is used.

From (3.84) $T_w(z)$ is obtained by numerical integration as

$$T_w(z) = T_s - \Delta T_d + \int_0^z F(z) dz \quad (3.85)$$

$T_c(z)$ is then obtained from (3.82).

Then, the average nodal temperature becomes

$$T_{cn} = \frac{(T_s - \Delta T_d + T_{ni}) \cdot \Delta z_{dk}}{2 \Delta z_n} + \frac{1}{\Delta z_n} \int_0^{\Delta z_n} T_c(z) dz \quad (3.86)$$

b) Case with Boiling Boundary

The case is depicted in fig. 3.7. The boiling boundary location, point D, is obtained from eqs. (3.84) and (3.82) by finding the value of $z = z_B$ which gives $T_c(z_B) = T_w(z_B) = T_s$. Then, the distance of boiling boundary to node entrance is given by

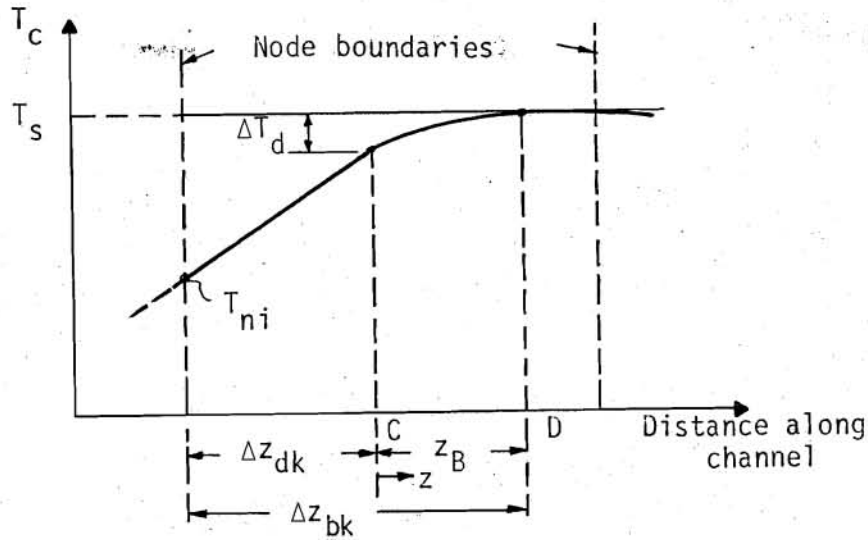


Figure 3.7:

Channel without Border Zone. Node with Bubble Detachment Point (C) and with Boiling Boundary (D)

$$\Delta z_{bk} = z_B + \Delta z_{dk} \quad (3.87)$$

The average nodal temperature is given by

$$T_{cn} = \frac{(T_s - \Delta T_d + T_{ni}) \Delta z_{dk}}{2 \Delta z_n} + \frac{T_s (\Delta z_n - \Delta z_{bk})}{\Delta z_n} + \frac{1}{\Delta z_n} \int_0^{\Delta z_{bk}} T_c(z) dz \quad (3.88)$$

where $T_c(z)$ is to be obtained from eqs. (3.82) and (3.84).

● Nodes without the Bubble Detachment Point

a) Case without Boiling Boundary

The case is depicted in fig. 3.8. The true quality distribution within the node is given by eq. (3.30).

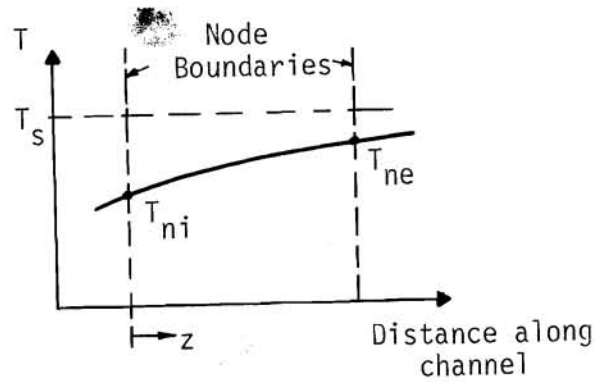


Figure 3.8:
 Channel without Border Zone.
 Node with Subcooled Boiling,
 without Bubble Detachment
 Point and without Boiling
 Boundary

Then,

$$\frac{dx_t}{dz} = \xi_n - \xi_n \exp\left(\frac{x_{ni}}{x_d} + \frac{\xi_n}{x_d} z - 1\right) \quad (3.89)$$

where ξ_n is defined by eq. (3.25).

Introducing (3.89) into (3.80) yields

$$\begin{aligned} dT_w = & \frac{1}{h_w^T [1 - x_{ni} - \xi_n z + x_d \exp(\frac{x_{ni}}{x_d} + \frac{\xi_n}{x_d} z - 1)]} \left\{ \frac{V_n P_n}{G_k \Delta z_n} - \frac{A_k}{G_k} [\rho'' h''^P + h'' \rho''^P + \right. \\ & + (1 - \alpha_n)(\rho_w^P h_w + \rho_w h_w^P) - 1] \dot{p} - [h_{sw} + h_w^T (T_s - T_w(z))] [1 - \exp(\frac{x_{ni}}{x_d} + \frac{\xi_n}{x_d} z - 1)] \xi_n - \\ & \left. - [(x_{ni} + \xi_n z - x_d \exp(\frac{x_{ni}}{x_d} + \frac{\xi_n}{x_d} z - 1)) (h''^P - h_w^P) + h_w^P] p_{zn} \right\} \quad (3.90) \end{aligned}$$

from which $T_w(z)$ is obtained by numerical integration. Then, eq. (3.82) gives $T_c(z)$ as

$$T_c(z) = T_w(z)[1-x_t(z)] + T_s x_t(z) \quad (3.91)$$

Then, the average nodal temperature is given by

$$T_{cn} = (1/\Delta z_n) \int_0^{\Delta z_n} T_c(z) dz \quad (3.92)$$

b) Case with Boiling Boundary

The case of shown in fig. 3.9. The boiling boundary location D is obtained from eqs. (3.90) and (3.91) by finding the value of $z=z_B$, so that $T_c(z_B)=T_w(z_B)=T_s$. Then, the distance of boiling boundary to node entrance is given by

$$\Delta z_{bk} = z_B \quad (3.93)$$

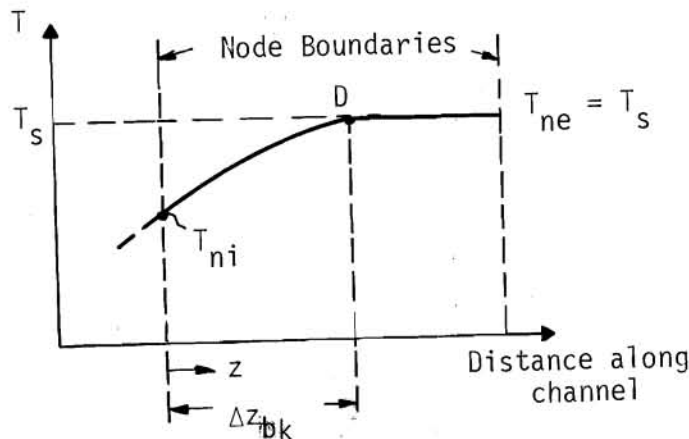


Figure 3.9:

Channel without Border Zone.
Node with Subcooled Boiling, without
Bubble Detachment Point and with
Boiling Boundary (D)

The nodal average temperature is obtained from

$$T_{cn} = \frac{1}{\Delta z_n} \int_0^{\Delta z_{bk}} T_c(z) dz + \frac{(\Delta z_n - \Delta z_{bk}) T_s}{\Delta z_n} \quad (3.94)$$

c) Nodes with Normal Boiling

These are the nodes that lie downstream of the boiling boundary. Their nodal temperatures are given by

$$T_{cn} = T_s \quad (3.95)$$

3.5.1.2 Channels with Border Zone

Let us assume that a border zone is present in nodes n_1 and n_1+1 .

● Nodes with Single-Phase Flow

Coolant temperatures of the nodes from channel entrance up to index n_1-1 are calculated by using eqs. (3.75)-(3.77).

If the bubble detachment point is in node n_1+1 , n_1 'th node also has single phase flow. That temperature at the border zone entrance is obtained from (3.14). The nodal temperature is given by

$$T_{cn} = \frac{T_{Bzi} + T_{cni}}{2} \left(\frac{\Delta z_n - \frac{\Delta z_n^-}{2}}{\Delta z_n} \right) + \frac{1}{\Delta z_n} \left\{ T_{Bzi} \frac{\Delta z_n^-}{2} + \frac{A_{tk} (P_{n+1} - P_n)}{6h_w^T G_k \Delta z_n^-} \left(\frac{\Delta z_n^-}{2} \right)^3 + \frac{A_{tk} P_n}{2h_w^T G_k} \left(\frac{\Delta z_n^-}{2} \right)^2 \right\} \quad (3.96)$$

● Nodes with Subcooled Boiling

- Bubble Detachment Point in n_1+1 'th Node

The case is shown in fig. 3.10. If the bubble detachment point is in node n_1+1 , the n_1 'th node has only single phase flow and (3.96) is valid. The following temperature distribution is valid within the one-phase flow part of the border zone:

$$T_{Bz}(z) = T_{Bzi} + \int_0^z \frac{A_{tk} P(z)}{h_w^T G_k} dz \tag{3.97}$$

$$= T_{Bzi} + \frac{A_{tk} (P_{n_1+1} - P_{n_1})}{2 h_w^T G_k \Delta z^-} z^2 + \frac{A_{tk} P_{n_1}}{h_w^T G_k} z$$

The temperature at the node exit is obtained from (3.97) by substituting $z = \Delta z^- / 2$.

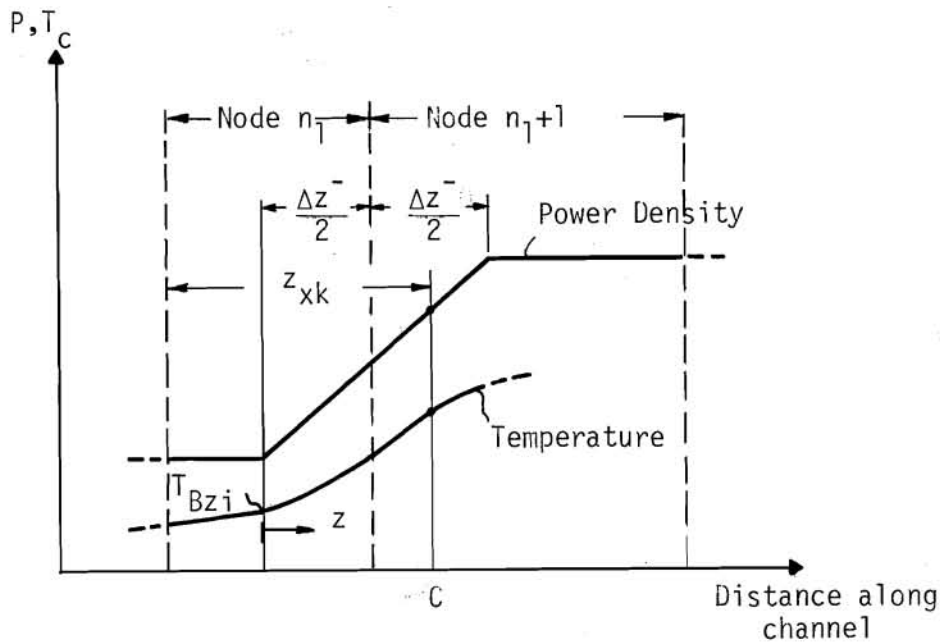


Figure 3.10:

Channel with Border Zone. Node with Subcooled Boiling. Bubble Detachment Point (C) in Node n_1+1

The temperature up to point C is also given by (3.97). At point C, both vapor and liquid water temperatures are equal to $T_s - \Delta T_d(z_{xk})$. Beyond point C, eqs. (3.80) and (3.82) will be used to obtain $T_w(z)$ and $T_c(z)$. The true quality distribution within the border zone is given by (3.37); hence,

$$\frac{dx_t(z)}{dz} = \eta_2 + 2\eta_1 z - x_d \left(\frac{2\eta_1}{x_d} z + \frac{\eta_2}{x_d} \right) \exp\left(\frac{\eta_1}{x_d}(z^2 - z_{xk}^2) + \frac{\eta_2}{x_d}(z - z_{xk})\right) \quad (3.98)$$

where z is measured from the beginning of the border zone. On the other hand,

$$q = A_{tk} p(z)$$

Then, eq. (3.80) gives

$$\begin{aligned} \frac{dT_w}{dz} = & \left\{ \frac{A_{tk} p(z)}{G_k} - [h_{sw} + h_w^T (T_x - T_w(z))] \frac{dx_t}{dz} - [x_t(z) h^{nP} + (1-x_t(z)) h_w^P] p_{zn} - \right. \\ & \left. - \frac{A_k}{G_k} [\rho^h h^{nP} + h^p \rho^{nP} + (1-\alpha_{n+1}) (\rho_w^p h_w^p + \rho_w^h h_w^p) - 1] p \right\} / (1-x_t(z)) h_w^T \end{aligned} \quad (3.99)$$

which is to be integrated from $z=z_{xk}$ to z ($z \leq \Delta z^-$) to obtain $T_w(z)$.

Then,

$$T_c(z) = T_w(z) [1-x_t(z)] + T_s x_t(z) \quad (3.100)$$

If $T_w(z_B) = T_s$ is reached before the end of the border zone is reached

$$T_{cn+1} = \frac{1}{\Delta z_{n+1}} \int_{\frac{\Delta z^-}{2}}^{z_{xk}} T_{Bz}(z) dz + \frac{1}{\Delta z_{n+1}} \int_{z_{xk}}^{z_B} T_{cn+1}(z) dz + \frac{(\Delta z_{n+1} - \Delta z_{bk}) T_s}{\Delta z_{n+1}} \quad (3.101)$$

where $T_{cn+1}(z)$ is calculated from (3.99) and (3.100). If this is the case, $T_{ci}=T_s$ for nodes with $i \geq n_1+2$ in the channel.

If $T_w(z) < T_s$ at the end of the border zone, continue integrating (3.80) in the remaining part of the node. Now, eq. (3.48),

$$q = (P_{n+1}V_{n+1})/(\Delta z_{n+1}) \quad (3.102)$$

and

$$dx_t/dz = \xi - \xi \exp[(x_{Bze}/x_d) + (\xi/x_d)z' - 1] \quad (3.103)$$

should be used in eq. (3.80).

If $T_w(z'=z_B)=T_s$ is reached before the node exit

$$T_{cn+1} = \frac{1}{\Delta z_{n+1}} \int_{\frac{\Delta z}{2}}^{z_{xk}} T_{Bz}(z) dz + \frac{1}{\Delta z_{n+1}} \int_{z_{xk}}^{\Delta z} T_{cn+1}(z) dz + \frac{1}{\Delta z_{n+1}} \int_0^{z_B} T_{cn+1}(z') dz' + \frac{(\Delta z_{n+1} - \Delta z_{bk})T_s}{\Delta z_n} \quad (3.104)$$

If this is the case, $T_{ci} = T_s$ for nodes with $i \geq n_1+2$ in the channel.

If $T_w(z') < T_s$ at the node exit, T_{cn+1} is found by using the equation

$$T_{cn+1} = \frac{1}{\Delta z_{n+1}} \int_{\frac{\Delta z}{2}}^{z_{xk}} T_{Bz}(z) dz + \frac{1}{\Delta z_{n+1}} \int_{z_{xk}}^{\Delta z} T_{cn+1}(z) dz + \frac{1}{\Delta z_{n+1}} \int_0^{\Delta z_{n+1} - \frac{\Delta z}{2}} T_{cn+1}(z') dz' \quad (3.105)$$

- Bubble Detachment Point in Node n_1

a) Node n_1 :

The case is depicted in fig. 3.11. The temperature at border zone entrance is obtained from (3.14). The temperature distribution between B and C is given by (3.97). The true quality distribution in the border zone is given by (3.37); hence (3.97), (3.98) and (3.99) are valid. Integrating (3.99) from $z = z_{xk}$ to z ($z \leq \frac{\Delta z^-}{2}$) gives $T_w(z)$.

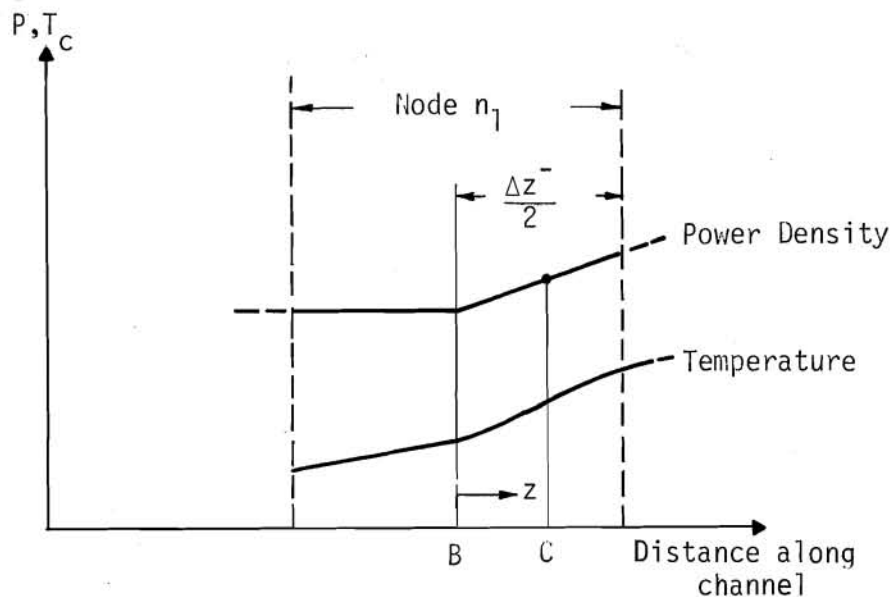


Figure 3.11:

Channel with Border Zone. Node with Subcooled Boiling. Bubble Detachment Point (C) in Node n_1 . Temperature Profile in Node n_1

Then, $T_c(z) = T_w(z) [1-x_t(z)] + T_s x_t(z)$.

If $T_w(z_B) = T_s$ is reached before the node exit

$$T_{cn} = \frac{(T_{n1i} + T_{Bzi}) (\Delta z_{n1} - \frac{\Delta z^-}{2})}{2 \Delta z_{n1}} + \frac{1}{\Delta z_{n1}} \int_0^{z_{xk}} T_{Bz}(z) dz +$$

$$+ \frac{1}{\Delta z_{n1}} \int_{z_{xk}}^{z_B} T_{cn1}(z) dz + \frac{(\Delta z_{n1} - \Delta z_{bk}) T_s}{\Delta z_{n1}} \quad (3.106)$$

If so, $T_{ci} = T_s$ for $i \geq n_1+1$.

If $T_w(\frac{\Delta z^-}{2}) < T_s$,

$$T_{cn} = \frac{(T_{n_1 i} + T_{Bzi})(\Delta z_{n_1} - \frac{\Delta z^-}{2})}{2 \Delta z_{n_1}} + \frac{1}{\Delta z_{n_1}} \int_0^{z_{xk}} T_{Bz}(z) dz + \frac{1}{\Delta z_{n_1}} \int_{z_{xk}}^{\frac{\Delta z^-}{2}} T_{cn}(z) dz \quad (3.107)$$

b) Node n_1+1 :

The case is shown in fig. 3.12. The true quality distribution in the border zone is given by (3.37). Therefore, eqs. (3.97), (3.98) and (3.99) are valid also in this case. Integrate (3.99) from $z = \Delta z^-/2$ to $z(z \leq \Delta z^-)$ to obtain $T_w(z)$ and $T_{cn+1}(z)$.

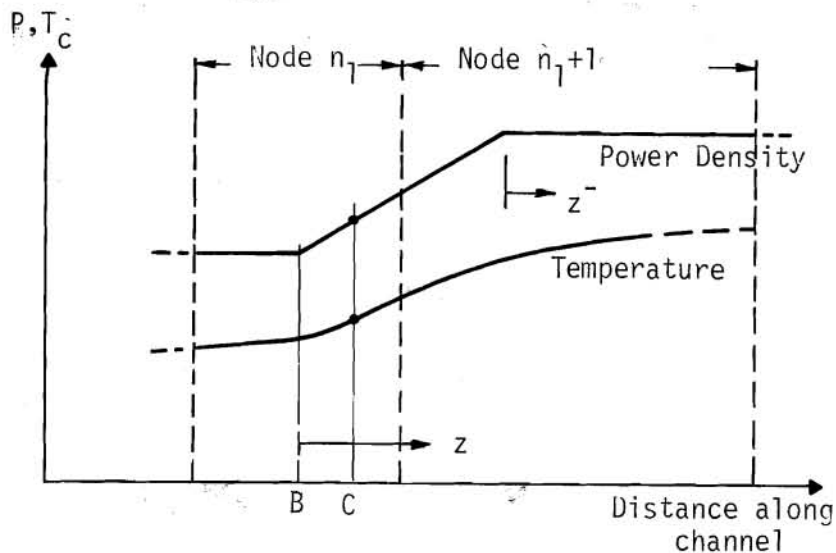


Figure 3.12:

Channel with Border Zone. Node with Subcooled Boiling. Bubble Detachment Point (C) in Node n_1 . Temperature Profile in Node n_{1+1}

If $T_w(z_B) = T_s$ is reached before the end of border zone

$$T_{cn+1} = \frac{1}{\Delta z_{n_1+1}} \int_{\frac{\Delta z^-}{2}}^{z_B} + \frac{(\Delta z_{n_1+1} - \Delta z_{bk}) T_s}{\Delta z_{n_1+1}} dz \quad (3.108)$$

Then, $T_{ci} = T_s$ for $i \geq n_1+2$.

If $T_w(\Delta z^-) < T_s$, then continue integrating (3.80) in the remaining part of the node. Now, eq. (3.48) and $q = V_{n_1+1} P_{n_1+1} / \Delta z_{n_1+1}$ should be used in (3.80).

If $T_w(z'=z_B) = T_s$ is reached before the end of node

$$T_{cn+1} = \frac{1}{\Delta z_{n+1}} \int_{\frac{\Delta z^-}{2}}^{\Delta z^-} T_{cn+1}(z) dz + \frac{1}{\Delta z_{n+1}} \int_0^{z_B} T_{cn+1}(z) dz + \frac{(\Delta z_{n+1} - \Delta z_{bk}) T_s}{\Delta z_{n+1}} \quad (3.109)$$

and $T_{ci} = T_s$ for $n \geq n_1+2$.

If T_w at $z' = \Delta z_{n+1} - (\Delta z^- / 2)$ is less than T_s , then

$$T_{cn+1} = \frac{1}{\Delta z_{n+1}} \int_{\frac{\Delta z^-}{2}}^{\Delta z^-} T_{cn+1}(z) dz + \frac{1}{\Delta z_{n+1}} \int_0^{\Delta z_{n+1} - \frac{\Delta z^-}{2}} T_{cn+1}(z) dz \quad (3.110)$$

c) Nodes Downstream of n_1+1

Eqs. (3.89) - (3.94) are valid in this case until the boiling boundary is passed. After the boiling boundary is passed eq. (3.95) is valid.

3.5.2 Calculations at the Working Point

At the working point $\dot{p} = 0$. The equations for calculations at the working point are obtained from those for transient calculations by setting $\dot{p} = 0$.

3.6 Nodal Fuel Temperature Distribution

Starting from the steady state Fourier heat conduction equation and assuming that the heat conduction coefficient λ_F varies with the radial fuel rod temperature $T_F(r)$ according to the relation

$$\lambda_F[T_F(r)] = \lambda_{Fc} / [1 + c_{\lambda}^T T_F(r)] \quad (3.111)$$

one obtains

$$T_{Fn} = \begin{cases} T_{Fsn} + (T_{Fsn} + 1/c_{\lambda}^T) (e^{c_{Fpn}} - c_{Fpn} - 1) / c_{Fpn} & \text{if } c_{Fpn} \text{ not } \ll 1 \\ T_{Fsn} + (1/2 c_{Fpn}) [T_{Fsn} + 1/c_{\lambda}^T + (1/3 c_{\lambda}^T) c_{Fpn}] & \text{if } c_{Fpn} \ll 1 \end{cases} \quad (3.112)$$

where T_{Fsn} is the nodal fuel surface temperature, c_{Fpn} is a dimensionless parameter defined as

$$c_{Fpn} = (1 - \varepsilon_F) r_{an}^2 P_n C_{\lambda}^T / (4 \varepsilon_{vF} \lambda_{Fc})$$

and ε_F is the percentage heat power which is lost directly through γ -radiation to the coolant and to the structure ($\varepsilon_F \cong 0.05$).

The fuel surface temperatures T_{Fsn} and the casing temperatures T_{Fcn} are obtained from the heat transfer condition as

$$T_{Fsn} = T_{cn} + (1 - \varepsilon_F) r_{an} P_n / (2 \alpha_{Fn} \varepsilon_{vF}) \quad (n=1, \dots, N) \quad (3.113)$$

$$T_{Fcn} = T_{cn} + (1 - \varepsilon_F) r_{ci} P_n / (2 \alpha_{cn} \varepsilon_{vF}) \quad (n=1, \dots, N) \quad (3.114)$$

with the overall heat transfer coefficients

$$\frac{1}{\alpha_{Fn}} = \frac{1}{\alpha_{wcn}} \frac{r_a}{r_{ca}} + \frac{1}{\lambda_c} r_a \ln \frac{r_{ca}}{r_{ci}} + \frac{1}{\alpha_G} \quad (3.115)$$

$$\frac{1}{\alpha_{cn}} = \frac{1}{\alpha_{wcn}} \frac{r_{ci}}{r_{ca}} + \frac{1}{\lambda_c} r_{ci} \ln \frac{r_{ca}}{r_{ci}} \quad (3.116)$$

where

- α_{wcn} = nodal heat transfer coefficient from canning to coolant,
- α_G = nodal heat transfer coefficient from fuel surface through the gap to canning,
- λ_c = heat conductivity through the canning and
- r_{ca}, r_{ci} = outer and inner radii of the canning.

The values of α_{wcn} are different for nodes with one- and two-phase flow such that

$$\begin{aligned} \alpha_{wcn} &= \alpha_{wcn,1} && \text{if } n=(k-1)n_z+1, \dots, (k-1)n_z+n_{dk} \\ \alpha_{wcn} &= \alpha_{wcn,2} && \text{if } n=(k-1)n_z+n_{dk}+2, \dots, kn_z \\ \alpha_{wcn} &= [\alpha_{wcn,1} \Delta z_{dk} + \alpha_{wcn,z} (\Delta z_n - \Delta z_{dk})] \Delta z_n && \text{if } n=(k-1)n_z+n_{dk}+1 \\ &&& (k=1, \dots, n_{xy}) \end{aligned} \quad (3.117)$$

The above equations are used in transient calculations as well as calculations at the working point.

3.7 System Pressure

Consider the top plenum, shown in fig. 3.13 schematically. The total saturated steam and the total saturated water entering the plenum are given by

$$G_{SH} = \sum_{k=1}^{n_{xy}} G_k X_{knze} \quad (3.118)$$

$$G_{WH} = \sum_{k=1}^{n_{xy}} (G_k - G_k X_{knze}) = G_E - G_{SH} = G_{WDE} + G_{FW} - G_{SH} \quad (3.119)$$

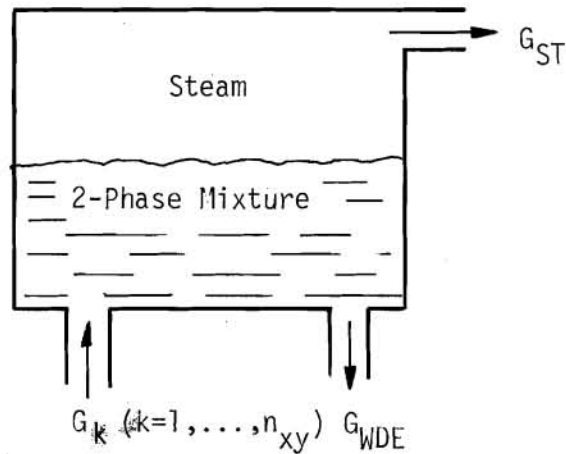


Figure 3.13:
Model of the Top Plenum

where $G_E = \sum_{k=1}^{n_{xy}} G_k$ is substituted in eq. (3.119) by assuming that quasi-static conditions apply.

Writing the mass and energy balance equations for the control volume defined by the plenum results in the following expressions for pressure p and water volume V_{WT} in the plenum:

$$\dot{p} = (\epsilon_1 - \epsilon_2) G_{SH} - \epsilon_1 G_{ST} + \epsilon_2 G_{FW} \quad (3.120)$$

$$\dot{V}_{WT} = \frac{1}{\rho' - \rho''} [G_{FW} - G_{ST}] - \theta_1 \dot{p} \quad (3.121)$$

where

$$\theta_1 = \frac{1}{\rho' - \rho''} [\rho' P_{WT} + \rho'' P (V_T - V_{WT})] \quad (3.122)$$

$$\epsilon_1 = \rho' h_{sw} / (\ell_1 V_{WT} + \ell_2 V_T) \quad (3.123)$$

$$\epsilon_2 = \epsilon_1 \cdot \rho'' / \rho' \quad (3.124)$$

with

$$\ell_1 = h_{sw} (\rho' P \rho'' - \rho'' P \rho') + (\rho' - \rho'') (h' P \rho' - h'' P \rho'') \quad (3.125)$$

$$\ell_2 = h_{sw} \rho' \rho'' P + (\rho' - \rho'') (h'' P \rho'' - 1) \quad (3.126)$$

Transient behaviours of p and V_{WT} are obtained from

$$p_F = p_B + \frac{1}{2} (\dot{p}_B + \dot{p}_F) \Delta t \quad (3.127)$$

$$V_{WTF} = V_{WTB} + \frac{1}{2} (\dot{V}_{WTB} + \dot{V}_{WTF}) \Delta t \quad (3.128)$$

where Δt is the time step that is used during the transient calculations, and the subscripts B and F refer to parameter values at the beginning and the end of a time step respectively. The derivative terms in these equations are evaluated by using eqs. (3.120) and (3.121).

3.8 Water Level in Top Plenum

Two options are available in the model to calculate the water level in the top plenum. In both cases the average steam quality x_T in the two-phase portion of the top plenum is assumed to be equal to the weighted average of the steam qualities of the flows entering the plenum. That is,

$$x_T = G_{SH} / G_E \quad (3.129)$$

and the average void fraction γ_T of the two-phase mixture in the top plenum is obtained from the Bankoff two-phase correlation using x_T .

In addition, the water volume and water level at the working point are assumed to be given. Then, the free water surface area A_T is estimated from

$$A_T = \frac{V_{WT}}{z_{WL}(1-\gamma_T)} \quad (3.130)$$

working point.

- Option I (IWLDY = 0)

In this option the following quasistatic equation is used to estimate the transient water level:

$$z_{WL} = \frac{V_{WT}}{A_T(1-\gamma_T)} \quad (3.131)$$

Here, z_{WL} , V_{WT} and γ_T are the current values and A_T is as calculated by eq. (3.130).

- Option II (IWLDY = 1)

This option represents another approximate but more sophisticated approach and includes the condensation and flashing effects due to pressure changes.

Mass balance for the volume which changes in time and lies below the water surface requires that

$$A_T z_{WL} \frac{d}{dt} [\rho'(1-\gamma_T) + \rho''\gamma_T] + \dot{z}_{WL} A_T [\rho'(1-\gamma_T) + \rho''\gamma_T] = G_{SH} + G_{WH} - G_{WDE} - G_{ST1} \quad (3.132)$$

where G_{ST1} is the steam mass flow rate passing from the two-phase mixture to the plenum top where only steam exists.

Energy balance for the volume that lies below the water surface gives

$$\begin{aligned} A_T z_{WL} \frac{d}{dt} [\rho' h' (1-\gamma_T) + \rho'' h'' \gamma_T - p] + \dot{z}_{WL} A_T [\rho' h' (1-\gamma_T) + \rho'' h'' \gamma_T - p] = \\ = h' (G_{WH} - G_{WDE}) + h'' (G_{SH} - G_{ST1}) \end{aligned} \quad (3.133)$$

Multiplying (3.132) by h'' and subtracting from (3.133), and arranging the terms result in

$$[\rho' (1-\gamma_T) h_{sw} + p] \dot{z}_{WL} - z_{WL} \beta_1 \dot{p} - z_{WL} \rho' h_{sw} \dot{\gamma}_T = (G_{FW} - G_{SH}) \frac{h_{sw}}{A_T} \quad (3.134)$$

In order to avoid $\dot{\gamma}_T$ -term in the above equation following modifications are introduced. First, note that

$$\begin{aligned} \frac{d}{dt} \{ [\rho' (1-\gamma_T) h_{sw} + p] z_{WL} \} = [\rho' (1-\gamma_T) h_{sw} + p] \dot{z}_{WL} + z_{WL} \dot{p} + \\ + z_{WL} \rho'^P (1-\gamma_T) h_{sw} \dot{p} - z_{WL} \rho' h_{sw} \dot{\gamma}_T - z_{WL} \rho' \gamma_T (h''^P - h'^P) \dot{p} \end{aligned} \quad (3.135)$$

Making use of eq. (3.135) to eliminate $\dot{\gamma}_T$ from eq. (3.134) gives

$$\frac{d}{dt}(Z) = (G_{FW} - G_{SH}) \frac{h_{sw}}{A_T} + z_{WL} \beta \dot{p} \quad (3.136)$$

where

$$Z = [\rho' (1-\gamma_T) h_{sw} + p] z_{WL} \quad (3.137)$$

and

$$\beta = (\rho'' - \rho') \gamma_T h''^P + \rho' h'^P \quad (3.138)$$

During transient calculations, first the value of Z is determined and then z_{WL} is estimated from eq. (3.137). Transient behavior of Z is obtained by using the following expression

$$Z_F = Z_B + \frac{1}{2} (\dot{Z}_B + \dot{Z}_F) \Delta t \quad (3.139)$$

where the time derivatives are calculated from eq. (3.136).

3.9 Feed Water and Outlet Steam Flow Rates and Water Volume in Top Plenum when Pressure is Controlled (Water Level is Constant)

3.9.1 Feed Water and Outlet Steam Flows are not Prescribed

If system pressure is controlled and if the water level in the top plenum is kept constant, then the corresponding feed water and outlet steam flows are calculated as follows.

Mass and energy balance equations written for the top plenum volume has yielded eqs. (3.120) and (3.121).

In addition,

$$\dot{p} = \frac{\Delta p}{\Delta t} \quad (3.140)$$

● Option I (IWLDY = 0)

In this case,

$$z_{WL} = \frac{V_{WT}}{A_T(1-\gamma_T)} \quad (3.141)$$

or in differential form

$$\dot{V}_{WT} = -A_T z_{WL} \dot{\gamma}_T = -A_T z_{WL} \frac{\Delta \gamma_T}{\Delta t} \quad (3.142)$$

where $\Delta\gamma_T$ is the change in the void fraction of 2-phase fluid in top plenum during the time step of length Δt .

Substituting (3.140) and (3.142) into (3.120) and (3.121) and solving for G_{ST} and G_{FW} yield

$$G_{ST} = G_{SH} + \frac{\epsilon_2(\rho' - \rho'')\theta_1^{-1}}{(\epsilon_1 - \epsilon_2)} \left(\frac{\Delta p}{\Delta t}\right) - \frac{\epsilon_2(\rho' - \rho'')}{\epsilon_1 - \epsilon_2} A_T z_{WL} \frac{\Delta\gamma_T}{\Delta t} \quad (3.143)$$

and

$$G_{FW} = G_{SH} + \frac{\epsilon_1(\rho' - \rho'')\theta_1^{-1}}{(\epsilon_1 - \epsilon_2)} \frac{\Delta p}{\Delta t} - \frac{\epsilon_1(\rho' - \rho'')}{(\epsilon_1 - \epsilon_2)} A_T z_{WL} \frac{\Delta\gamma_T}{\Delta t} \quad (3.144)$$

Calculation of V_{WT} is done from (3.121) according to

$$\Delta V_{WT} = \frac{1}{2} (\dot{V}_{WTB} + \dot{V}_{WTF}) \cdot \Delta t \quad (3.145)$$

● Option II (IWLDY = 1)

Writing the mass and energy balance for the control volume which lies under the free water surface in the top plenum, and then making the necessary operations yield

$$\beta_1 \dot{p} + \rho' h_{sw} \dot{\gamma}_T = \frac{h_{sw}}{A_T z_{WLW}} (G_{SH} - G_{FW}) \quad (3.146)$$

where

$$\beta_1 = (1 - \gamma_T)(\rho' h'^P - \rho'' h''^P_{sw}) + \gamma_T \rho'' h''^{P-1} \quad (3.147)$$

If $\Delta\gamma_T$ is the change in the void fraction of the two-phase fluid in top plenum during a time step Δt , one can write $\dot{\gamma}_T = \Delta\gamma_T / \Delta t$ into (3.146).

Solving for G_{FW} from (3.146) gives

$$G_{FW} = G_{SH} - \frac{A_T z_{WL} \beta_1}{h_{sw}} \frac{\Delta p}{\Delta t} - A_T z_{WL} \rho' \frac{\Delta \gamma_T}{\Delta t} \quad (3.148)$$

Substitute (3.148) into (3.120) and solve for G_{ST} to obtain

$$G_{ST} = G_{SH} - \left[\frac{A_T z_{WL} \beta_1 \epsilon_2^{-h_{sw}}}{h_{sw} \epsilon_1} \right] \frac{\Delta p}{\Delta t} - \frac{\epsilon_2 A_T z_{WL} \rho'}{\epsilon_1} \frac{\Delta \gamma_T}{\Delta t} \quad (3.149)$$

From (3.148) and (3.149)

$$G_{FW} - G_{ST} = - \left[\frac{A_T z_{WL} \beta_1 (\epsilon_1^{-\epsilon_2}) + h_{sw}}{h_{sw} \epsilon_1} \right] \frac{\Delta p}{\Delta t} - \left[\frac{A_T z_{WL} \rho' (\epsilon_1^{-\epsilon_2})}{\epsilon_1} \right] \frac{\Delta \gamma_T}{\Delta t} \quad (3.150)$$

Substitution of $G_{FW} - G_{ST}$ into (3.121) yields

$$\dot{V}_{WT} = - \left[\frac{A_T z_{WL} \beta_1 (\epsilon_1^{-\epsilon_2}) + h_{sw}}{(\rho' - \rho'') h_{sw} \epsilon_1} + \theta_1 \right] \frac{\Delta p}{\Delta t} - \left[\frac{A_T z_{WL} \rho' (\epsilon_1^{-\epsilon_2})}{\epsilon_1 (\rho' - \rho'')} \right] \frac{\Delta \gamma_T}{\Delta t} \quad (3.151)$$

from which ΔV_{WT} is calculated as

$$\Delta V_{WT} = \frac{1}{2} (\dot{V}_{WTB} + \dot{V}_{WTF}) \cdot \Delta t \quad (3.152)$$

3.9.2 Externally Prescribed Feedwater and Outlet Steam Flows

If system pressure is controlled, and if G_{ST} or G_{FW} is specified freely as a perturbation, then neither the water volume nor the water level in the top plenum can be kept constant. Moreover, both G_{ST} and G_{FW} cannot be specified simultaneously in a pressure controlled run.

If G_{FW} is specified, then G_{ST} is obtained from (3.120) as

$$G_{ST} = \frac{1}{\epsilon_1} [(\epsilon_1 - \epsilon_2) G_{SH} + \epsilon_2 G_{FW} - \dot{p}] \quad (3.153)$$

If G_{ST} is specified, the same equation yields

$$G_{FW} = - \frac{1}{\epsilon_2} [(\epsilon_1 - \epsilon_2) G_{SH} - \epsilon_1 G_{ST} - \dot{p}] \quad (3.154)$$

Water volume V_{WT} and water level z_{WL} are obtained as in sections 3.7 and 3.8.

3.10 Thermodynamic Properties

Thermodynamic properties of coolant water, which are available at the working point, are modified during the transient calculations according to the following expressions.

$$\begin{aligned} \rho' &= \rho'_w + \rho'^P \Delta p \\ \rho'' &= \rho'_w + \rho''^P \Delta p \\ h' &= h'_w + h'^P \Delta p \\ h'' &= h''_w + h''^P \Delta p \\ T_s &= T_{sw} + T_s^P \Delta p \\ h_{FW} &= h_{FWw} + h_w^T (T_{FW} - T_{FWw}) \\ \rho_E &= \rho_{Ew} + \rho_w^T (T_E - T_{Ew}) \\ h_E &= h_{Ew} + h_w^T (T_E - T_{Ew}) \end{aligned} \quad (3.155)$$

where Δp is the difference between the pressure at which the properties are desired and the pressure at the working point. Normally, the properties at the mean pressure during a time step are used in calculations unless a specific equation requires otherwise, e.g. equations (3.127), (3.128), (3.139).

4. XENON-IODINE DISTRIBUTION

Xenon-iodine dynamics are governed by the following set of differential equations:

$$\dot{X}_{e_n} = \gamma_x (\sum_{f1n} \phi_{1n} + \sum_{f2n} \phi_{2n}) - \lambda_x X_{e_n} + \lambda_I I_n - (\sum_{a1n}^x \phi_{1n} + \sum_{a2n}^x \phi_{2n}) X_{e_n} \quad (n = 1, \dots, N) \quad (4.1)$$

$$\dot{I}_n = \gamma_I \sum_{f2n} \phi_{2n} - \lambda_I I_n \quad (n = 1, \dots, N) \quad (4.2)$$

with the initial conditions $X_{e_n}(t=t_w) = X_{e_{nw}}$ and $I_n(t=t_w) = I_{nw}$ given at the working point t_w .

Introducing the expressions for ϕ_{1n} and ϕ_{2n} as given by eqs. (2.15) and (2.16) and defining the xenon absorption factor as

$$\Gamma_{nw} = (\epsilon_{nw} - 1) \sum_{a1n}^x / (\epsilon_{nw} \sum_{f1nw}) + \sum_{a2n}^x / (\epsilon_{nw} \sum_{f2nw}) \quad (n = 1, \dots, N) \quad (4.3)$$

eqs. (4.1) and (4.2) become

$$\dot{X}_{e_n} = \frac{\gamma_x}{E_{eff}} P_n - \left(\lambda_x + \frac{\Gamma_{nw}}{E_{eff}} P_n \right) X_{e_n} + \lambda_I I_n \quad (4.4)$$

$$\dot{I}_n = \frac{\gamma_I}{E_{eff}} P_n - \lambda_I I_n \quad (4.5)$$

The steady state xenon and iodine densities are obtained from the above two equations as

$$Xe_n = \frac{(\gamma_x + \gamma_I) P_n}{\lambda_{x,eff} + \Gamma_{nw} P_n} \quad (4.6)$$

$$I_n = \gamma_I P_n / (E_{eff} \lambda_I) \quad (4.7)$$

Transient calculations are carried out by using the following equations:

$$I_{nF} = I_{nB} + \frac{1}{2} (\dot{I}_{nB} + \dot{I}_{nF}) \Delta t \quad (n = 1, \dots, N) \quad (4.8)$$

$$Xe_{nF} = Xe_{nB} + \frac{1}{2} (\dot{Xe}_{nB} + \dot{Xe}_{nF}) \Delta t \quad (n = 1, \dots, N) \quad (4.9)$$

where the time derivatives are calculated from eqs. (4.1) and (4.2).

5. MODIFICATION OF POWER DENSITY DISTRIBUTION EQUATION

In principle, the core power density distribution may be solved from eqs. (2.35-2.39) by iteration. However, difficulties arise in practice due to the strong thermodynamic feedback effects, which deteriorate the convergence rate of recursion and even result in instability. This difficulty is greatly eliminated if those terms of $\delta_r L_n$ which are directly proportional to $\delta_r P_n$ are transferred to the left-hand side of the equation.

5.1 Power Feedback from the Coolant Temperature Term

The term $\delta_r T_{cn}$ in eqs. (2.37-2.39) is normally a function of a relatively large number of variables and affected by a change

in any one of them. Let us write $\delta_r T_{cn}$ in terms of two components as

$$\delta_r T_{cn} = \delta_r T_{cn,p} + \delta_r E_{cn} \quad (5.1)$$

Here, the term $\delta_r T_{cn,p}$ is the part of change in normalized T_{cn} due to a change only in normalized power distribution and can be estimated as follows by taking only the first order changes from the working point:

$$\delta_r T_{cn,p} = \sum_{j=(k-1)n_z+1}^{n+1} \Lambda_{nj} \delta_r P_j \quad (5.2)$$

where the coefficients Λ_{nj} are defined as in appendix 1.

During transient calculations, the value of $\delta_r E_{cn}$ corresponding to a time step is calculated not around the working point but from the following expression:

$$\delta_r E_{cn} = \frac{1}{T_{CN}} (T_{cnF} - T_{cnB}) \quad (5.3)$$

Here, T_{cnF} and T_{cnB} , which represent the values at the end and the beginning of a time step, are calculated from the nonlinear equations keeping the power terms P_n at their levels which exist at the beginning of time step but allowing the other variables to change.

5.2 Power Feedback from the Fuel Temperature Term

Taking the variations of eq. (3.112) and normalizing the terms one obtains

$$\delta_r T_{Fn} = S_{1n} \delta_r T_{cn} + S_{2n} \delta_r P_n \quad (n = 1, \dots, N) \quad (5.4)$$

where the coefficients S_{1n} and S_{2n} are evaluated at the working point and given by

$$S_{1n} = T_{CN} D_{TFwn} / T_{FN} \quad (n = 1, \dots, N) \quad (5.5)$$

$$S_{2n} = P_N D_{TFPn} / T_{FN} \quad (n = 1, \dots, N) \quad (5.6)$$

with

$$D_{TFwn} = 1 + C_{\lambda}^T \frac{(T_{Fnw} - T_{Fsnw})}{1 + C_{\lambda}^T T_{Fsnw}} \quad (5.7)$$

$$D_{TFPn} = C_{RF} \left(\frac{1 + C_{\lambda}^T T_{Fnw}}{1 + C_{\lambda}^T T_{Fsnw}} \right) + C_{TF} (1 + C_{\lambda}^T T_{Fnw}) - \frac{T_{Fnw} - T_{Fsnw}}{P_{nw}} \quad (5.8)$$

and

$$C_{RF} = \frac{r_a (1 - \epsilon_F)}{2 \alpha_{Fn} \epsilon_{VF}} \quad (5.9)$$

$$C_{TF} = \frac{r_a^2 (1 - \epsilon_F)}{4 \lambda_{FC} \epsilon_{VF}} \quad (5.10)$$

Substituting $\delta_r T_{cn}$ from eq. (5.1) into (5.4) gives

$$\delta_r T_{Fn} = S_{1n} \left[\sum_{j=(k-1)n_z+1}^{n+1} \Lambda_{nj} \delta_r P_j \right] + S_{2n} \delta_r P_n + \delta_r E_{Fn} \quad (5.11)$$

with $\delta_r E_{Fn} = S_{1n} \delta_r E_{cn}$.

The coefficients of the power terms in eq. (5.11) are evaluated at the working point. The term $\delta_r E_{Fn}$ is, however, interpreted as changes in normalized T_{Fn} due to changes of variables other than power. During transient calculations, the value of $\delta_r E_{Fn}$ corresponding to a time step is calculated not using a linear expression around the working point, but from the following expression:

$$\delta_{r E_{Fn}} = \frac{1}{T_{FN}} (T_{Fn,F} - T_{Fn,B}) \quad (5.12)$$

Here, $T_{Fn,F}$ and $T_{Fn,B}$ are calculated from the nonlinear equations keeping the nodal power density values at their levels which exist at the beginning of the time step, but allowing the other variables to change.

5.3 Power Feedback from the Void Fraction Term

The term $\delta_{r \alpha_n}$ in eqs. (2.37-2.39) is composed of two components as

$$\delta_{r \alpha_n} = \delta_{r \alpha_{np}} + \delta_{r E_{\alpha n}} \quad (5.13)$$

Here, the term $\delta_{r \alpha_{np}}$ is the part due to a change only in normalized power distribution and is calculated by considering only the first order changes from the working point as

$$\delta_{r \alpha_{np}} = \sum_{j=(k-1)n_z+1}^{n+1} W_{nj} \delta_{r P_j} \quad (5.14)$$

where the coefficients W_{nj} are defined as in appendix 2.

During transient calculations, the value of $\delta_{r E_{\alpha n}}$ corresponding to a time step is calculated not around the working point but from

$$\delta_{r E_{\alpha n}} = \frac{1}{\alpha_N} (\alpha_{nF} - \alpha_{nB}) \quad (5.15)$$

Here, α_{nF} and α_{nB} represent respectively the values at the end and the beginning of a time step, and are calculated from the non linear equations, keeping the power terms P_n at their values which exist at the beginning of the time step but allowing the other variables to change.

5.4 Modification of the Power Matrix

Substituting eqs. (5.1), (5.2), (5.4), (5.13) and (5.14) into (2.37) gives

$$\delta\eta_n = \delta\eta_{n1} + \delta F_{\eta n} \quad (n = 1, \dots, N) \quad (5.16)$$

where

$$\delta\eta_{n1} = \eta_{nw} \{ F_{xww}^{(n)} \delta_r X_{en} + F_{Fww}^{(n)} \delta_r E_{Fn} + F_{Cww}^{(n)} \delta_r E_{cn} + F_{Aww}^{(n)} \delta_r E_{an} + \sum_{r=1}^R F_{uww}^{(n,r)} \delta_r U_{nr} \} \quad (5.17)$$

and

$$\delta F_{\eta n} = [R_{\eta n}] [\delta_r P] = \sum_{j=1}^N R_{\eta n}(j) \delta_r P_j \quad (5.18)$$

where $[R_{\eta n}]$ is an N-dimensional vector whose elements are defined as

$$R_{\eta n}(j) = \eta_{nw} F_{Fww}^{(n)} \cdot S_{1n} \cdot \Lambda_{nj} + \eta_{nw} \cdot F_{Cww}^{(n)} \Lambda_{nj} + \eta_{nw} F_{Aww}^{(n)} W_{nj} \quad \text{for } j=(k-1)n_z+1, \dots, n-1 \text{ and } j=n+1 \quad (5.19a)$$

$$R_{\eta n}(j) = \eta_{nw} F_{Fww}^{(n)} \cdot S_{2n} + \eta_{nw} \cdot F_{Fww}^{(n)} S_{1n} \Lambda_{nj} + \eta_{nw} F_{Cww}^{(n)} \Lambda_{nj} + \eta_{nw} F_{Aww}^{(n)} W_{nj} \quad \text{for } j=n \quad (5.19b)$$

$$R_{\eta n}(j) = 0 \quad \text{for } j > n+1 \text{ or } j < (k-1)n_z+1 \quad (5.19c)$$

Similarly, substituting eqs. (5.1), (5.2), (5.4), (5.13) and (5.14) into (2.38) gives

$$\delta \Sigma_{aln} = \delta \Sigma_{aln,1} + \delta F_{aln} \quad (5.20)$$

with

$$\begin{aligned} \delta \Sigma_{aln,1} = & \sum_{al}^X X_{eN} \delta_r X_{e_n} + \sum_{al}^F T_{FN} \delta_r E_{Fn} + \sum_{al}^C T_{CN} \delta_r E_{Cn} + \\ & + \sum_{al}^D \rho_{\alpha N}^{\alpha} \delta_r E_{\alpha n} + \frac{1}{\Delta z_n} \sum_{r=1}^R C_{lnr} \Delta \Sigma_{alr}^U \delta U_{nr} \end{aligned} \quad (5.21)$$

and

$$\delta F_{aln} = [R_{aln}] [\delta_r P] = \sum_{j=1}^N R_{aln}(j) \delta_r P_j \quad (5.22)$$

where R_{aln} is an N-dimensional vector with elements defined as

$$R_{aln}(j) = \sum_{aln}^F T_{FN} S_{ln} \Lambda_{nj} + \sum_{aln}^C T_{CN} \Lambda_{nj} + \sum_{aln}^D \rho_{\alpha N}^{\alpha} W_{nj} \quad (5.23a)$$

for $j=(k-1)n_z+1, \dots, n-1$ and $j=n+1$

$$R_{aln}(j) = \sum_{aln}^F T_{FN} S_{2n} + \sum_{aln}^F T_{FN} S_{ln} \Lambda_{nj} + \sum_{aln}^C T_{CN} \Lambda_{nj} + \sum_{aln}^D \rho_{\alpha N}^{\alpha} W_{nj} \quad (5.23b)$$

for $j=n$

$$R_{aln}(j) = 0 \quad \text{for } j > n+1 \text{ or } j < (k-1)n_z+1 \quad (5.23c)$$

Substituting eqs. (5.1), (5.2), (5.4), (5.13) and (5.14) into (2.39) gives

$$\delta \Sigma_{12n} = \delta \Sigma_{12n,1} + \delta F_{12n} \quad (5.24)$$

with

$$\begin{aligned} \delta \Sigma_{12n,1} = & \sum_{12n} X_e \delta X_{eN} + \sum_{12n} T_{FN} \delta E_{FN} + \sum_{12n} T_{CN} \delta E_{CN} + \\ & + \sum_{12n} \rho^{\alpha} \delta E_{\alpha n} + \frac{1}{\Delta z_n} \sum_{r=1}^R C_{1nr} \Delta \Sigma_{12r} U_{CN} \delta U_{nr} \end{aligned} \quad (5.25)$$

and

$$\delta F_{12n} = [R_{12n}] [\delta_r P] = \sum_{j=1}^N R_{12n}(j) \delta_r P_j \quad (5.26)$$

where R_{12n} is an N -dimensional vector such that

$$R_{12n}(j) = \sum_{12n} T_{FN} S_{1n} \Lambda_{nj} + \sum_{12n} T_{CN} \Lambda_{nj} + \sum_{12n} \rho^{\alpha} \alpha_N W_{nj} \quad (5.27a)$$

for $j=(k-1)n_z+1, \dots, n-1$ and $j=n+1$

$$R_{12n}(j) = \sum_{12n} T_{FN} S_{1n} \Lambda_{nj} + \sum_{12n} T_{CN} \Lambda_{nj} + \sum_{12n} T_{FN} S_{2n} + \sum_{12n} \rho^{\alpha} \alpha_N W_{nj} \quad (5.27b)$$

for $j=n$

$$R_{12n}(j) = 0 \quad (5.27c)$$

for $j > n+1$ or $j < (k-1)n_z+1$

Substitute eqs. (5.16), (5.20) and (5.24) into (2.36) to obtain

$$\delta_{r,n} L = \delta_{r,n1} L + \delta_{r,NL} L + \delta_{r,Ln} F \quad (5.28)$$

where

$$\begin{aligned} \delta_{rLn} = & -(P_n/P_N)[\eta_n(\delta\Sigma_{a1n,1} + \delta\Sigma_{12n,1}) + (\Sigma_{a1nw} + \Sigma_{12nw} + W_{nw})\delta\eta_{n1}] + \\ & + \sum_{m=1}^{M_n} [(P_{n_m}/P_N)W_{n_m w} \delta\eta_{n_m 1}] \end{aligned} \quad (5.29)$$

$$\begin{aligned} \delta_{rFn} = & -(P_n/P_N)[\eta_{nw}(\delta F_{a1n} + \delta F_{12n}) + (\Sigma_{a1nw} + \Sigma_{12nw} + \omega_{nw})\delta F_{\eta n}] + \\ & + \sum_{m=1}^{M_n} [(P_{n_m}/P_N)\omega_{n_m w} \delta F_{\eta n_m}] \end{aligned} \quad (5.30)$$

and the nonlinear term

$$\delta_{rFn} = -(P_n/P_N)(\eta_n - \eta_{nw})(\delta F_{a1n} + \delta F_{12n}) \quad (5.31)$$

Substituting eqs. (5.18), (5.22) and (5.26) into (5.30) yields the following equation for δ_{rFn} :

$$\delta_{rFn} = [F_{FBTn}] [\delta_r P] = \sum_{j=1}^N F_{FBTnjw} \delta_{rPj} \quad (5.32)$$

where F_{FBTn} is an N-dimensional vector with the elements defined as

$$\begin{aligned} F_{FBTnjw} = & -(P_n/P_N)[\eta_{nw}(R_{a1n}(j) + R_{12n}(j)) + (\Sigma_{a1nw} + \Sigma_{12nw} + \omega_{nw})R_{\eta n}(j)] + \\ & + \sum_{m=1}^{M_n} (P_{n_m}/P_N)\omega_{n_m w} R_{\eta n_m}(j) \end{aligned} \quad (5.33)$$

Then, the power equation (2.35) becomes

$$\sum_{j=1}^N [(F_{pw})_{njw} - F_{FBTnjw}] \delta_r P_j = \delta_r L_{nl} + \delta_r F_{Nn} \quad (5.34)$$

which is the modified power density distribution equation.

6. RESULTS OF PRELIMINARY TESTS

6.1 The Computer Code GARLIC-B

Based on the model, the digital code GARLIC-B ("Garching Real-Time Core and Plant Model for BWR") was written. The development of the code itself has also been a major work and, therefore, is not included in the subject matter of this report¹). The details of the program structure, the arrangement of the input parameters and the form of the output are described in considerable detail in reference (Er et al. 81).

The code is aimed to be used on an on-site process computer in parallel to the actual reactors process. Thus, special measures had to be taken in order to increase the computational speed and reduce the computer storage. It is written in FORTRAN IV (H-Extended) language and tested on an AMDAHL 470/VI type of computer. In order to save memory space, variable dimensioning of the arrays is adopted and all arrays are stored into a pool vector whose portion is changed during different steps of the program execution. The variations in parameters during one time step are calculated by using multiple iteration loops. Separating the neutron and power kinetics from the xenon-iodine dynamics, treating the neutron kinetics and most of the thermohydrodynamics in a pseudo-stationary way, using coupling coefficients to describe the neutron diffusion, using superboxes,

¹) The code consists of some ninety subroutines some of which comprising as much as 2 000 lines.

taking advantage of symmetry properties of the core and applying sparse matrix technique for solving the algebraic power equation system help reducing the computation time of the code.

6.2 Preliminary Tests Results

Preliminary test runs show that the model and the corresponding code GARLIC-B is capable of calculating the transient behavior of BWR power plants, although the accuracy of the results needs to be tested yet. Five such runs are presented in Figures 6.1 - 6.5. A summary of the node partition and computational information about these runs are given in Table 6.1. These runs, especially those in which the system pressure is kept constant, seem to be quite encouraging and show that real-time calculations are feasible. At present, further test runs are carried out to test the model and the code under more severe perturbations. The initial phase of tests and further modifications of the code and the model are expected to continue for several months more.

7. FINAL REMARKS

The initial tests show that the model and the corresponding computer code are capable to compute in real time the operational transients of nuclear power plants with a BWR. Increasing the computational speed and reduction of computer storage were made possible by means of special measures such as separation of the neutron and power kinetics from xenon-iodine dynamics, treatment of neutron kinetics and most of thermo-hydrodynamics in a pseudo-stationary way, usage of coupling coefficients, combining coarse mesh elements into superboxes, taking advantage of symmetry properties of the core, making use of sparse matrix techniques and utilization of several recursion formulas adaptively. In order to improve computational efficiency, further modifications on the model and on the methods of calculation will be introduced when tests progress.

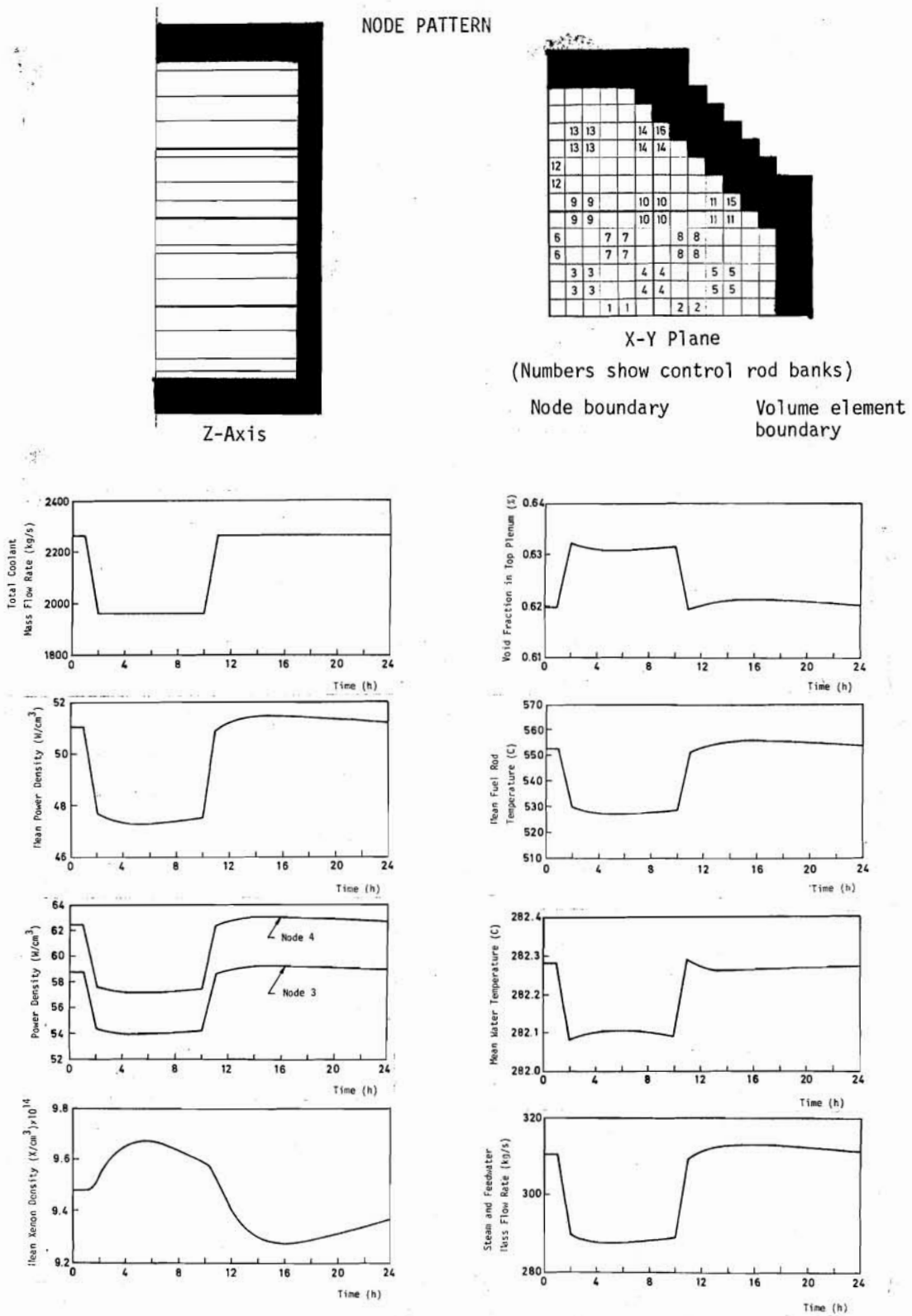


Figure 6.1:
 Transient Behavior of a BWR Nuclear Power Plant
 Coolant Mass Flow Changed
 (System Pressure Control, 1/4 Core, 16 Nodes)

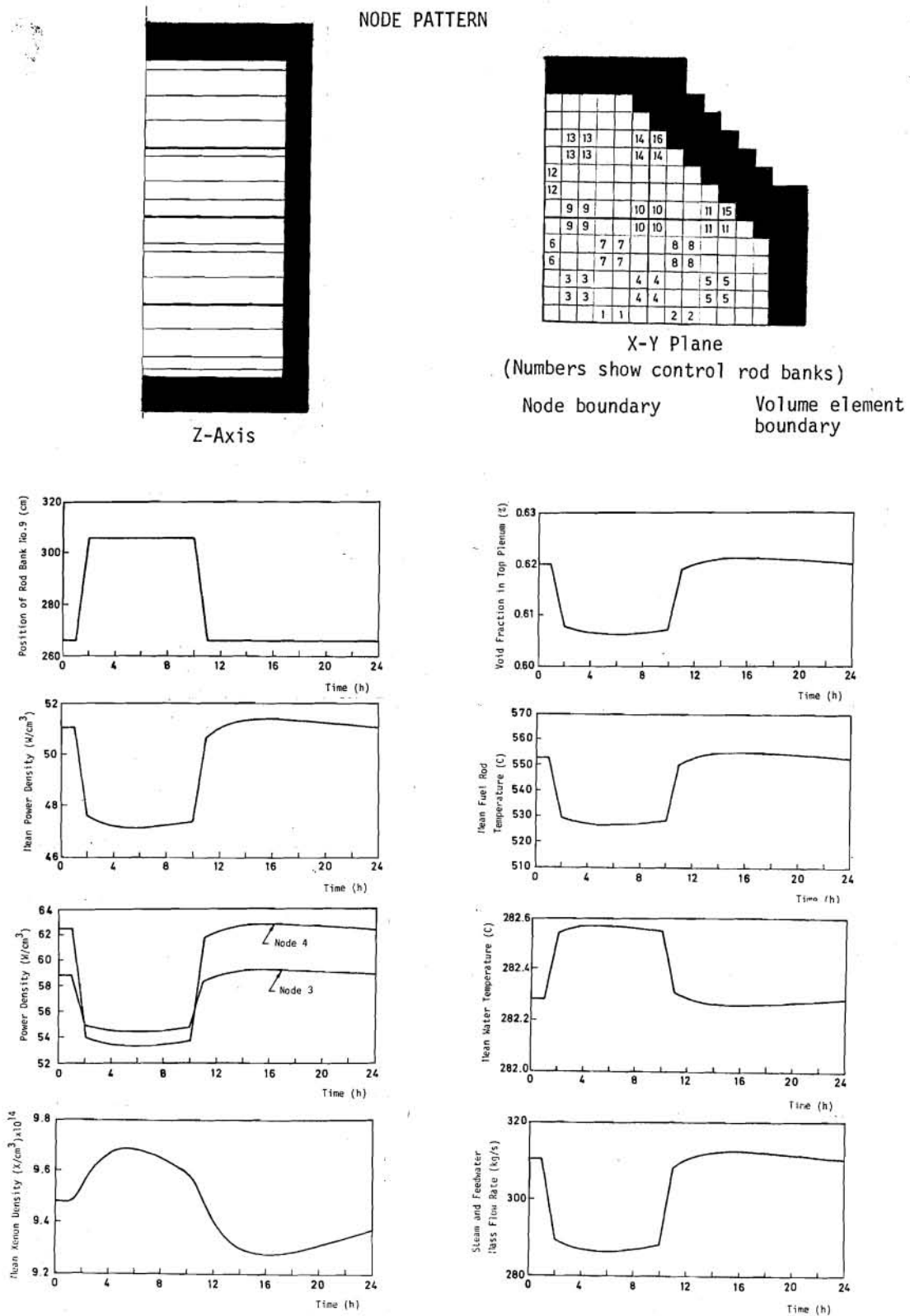


Figure 6.2:
 Transient Behavior of a BWR Nuclear Power Plant
 Control Rod Bank 9 Moved
 (System Pressure Control, 1/4 Core, 16 Nodes)

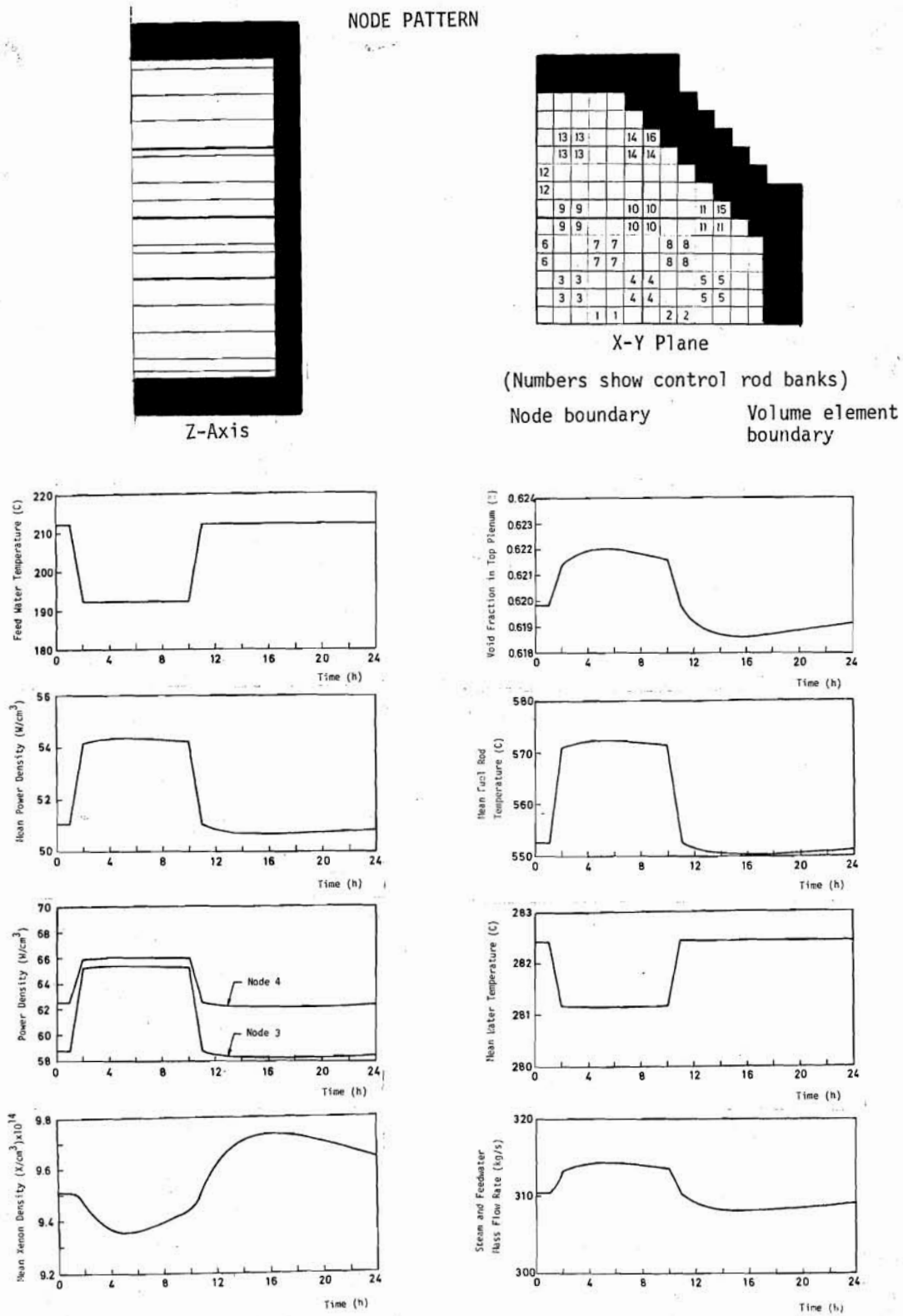


Figure 6.3:
 Transient Behavior of a BWR Nuclear Power Plant
 Feed Water Temperature Changed
 (System Pressure Control, 1/4 Core, 16 Nodes)

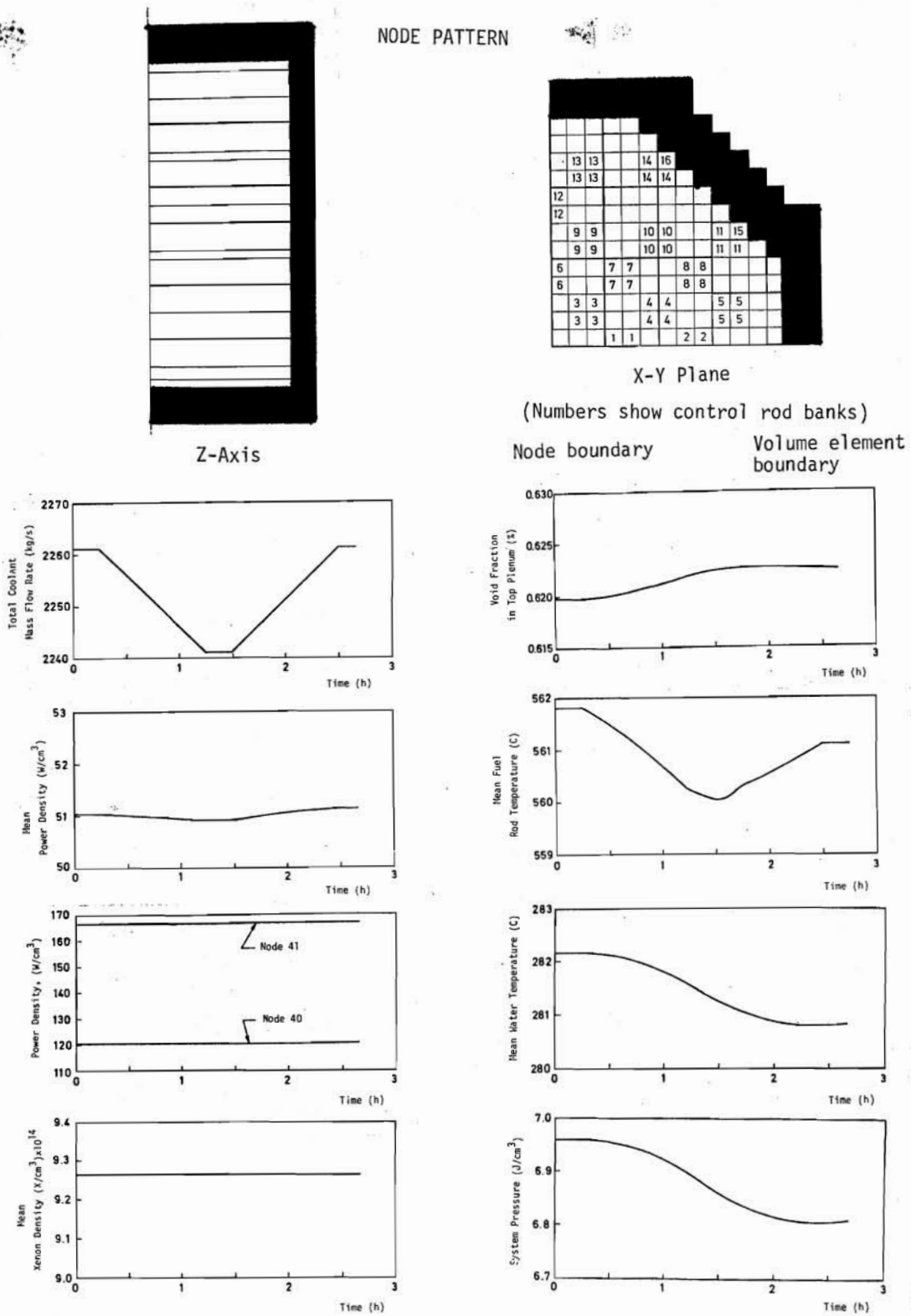


Figure 6.4:
 Transient Behavior of a BWR Nuclear Power Plant
 Coolant Mass Flow Changed
 (System Pressure Free, 1/4 Core, 96 Nodes)

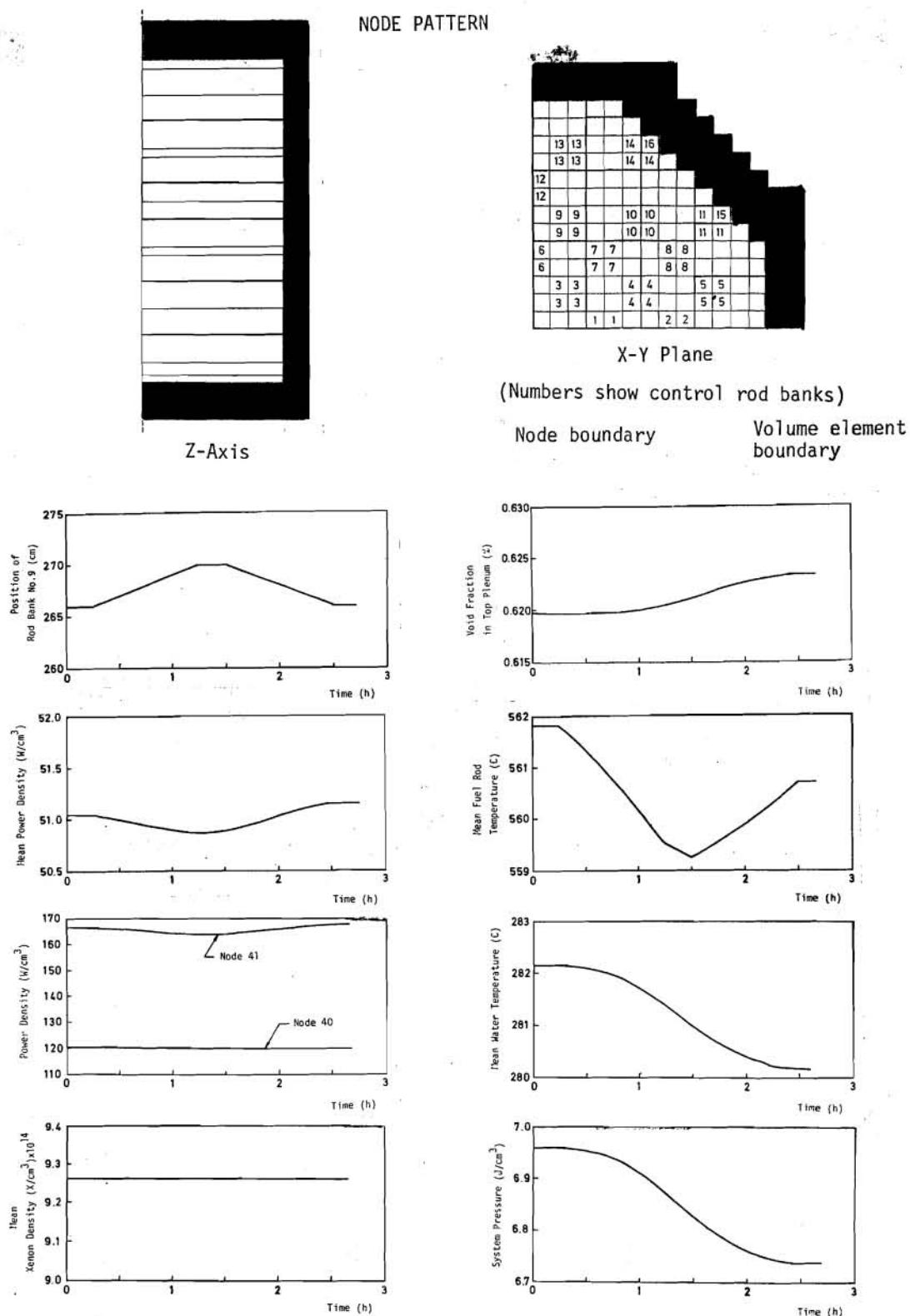


Figure 6.5:
 Transient Behavior of a BWR Nuclear Power Plant
 Control Rod Bank 9 Moved
 (System Pressure Free, 1/4 Core, 96 Nodes)

Tab. 6.1:
Computational Information about the Test Runs

Run	No. of Nodes	System Pressure	Perturbation	Run Duration [h:min]	Total CPU Time [s]	Total No. of Time Steps	Total No. of Iterations in the Outermost Loop
Figure 6.1	16	constant	G_E	24:00	35.98	72	1956
Figure 6.2	16	constant	Rod Bank 9	24:00	37.56	72	2157
Figure 6.3	16	constant	T_{FW}	24:00	34.55	72	1828
Figure 6.4	96	free	G_E	2:40	142.38	32	786
Figure 6.5	96	free	Rod Bank 9	2:40	120.46	32	699

The present tests aim to show the capability of the model and the corresponding code GARLIC-B to calculate the transient behavior of nuclear power plants with a BWR in real time. After these tests, accuracy of the calculations must be checked. Many parameters in the model, such as the coupling coefficients and the coefficient matrices in the power equation, are calculated using the working point data and kept at their original values throughout calculations. Since the model is in a way tuned to the working point it is expected to be quite accurate near this point. However, accuracy may be degraded if power level or distribution deviate largely from the working point. Therefore, the second phase of tests will involve transient runs starting from a working point and taking the system to a considerably different power level. Then, the state of the system at the newly reached power level will be checked against the results which would be obtained from the comprehensive codes (QUABOX/CUBBOX (La et al. 77a; 77b; 78) etc.).

The last phase of tests will involve post calculations of measured operational transients from actual nuclear power plants with a BWR.

REFERENCES

- (AT 80) Atomic Energy Research Establishment:
Subroutine NA28A, Version 15.4.80
Harwell Software Library,
AERE, Oxfordshire, UK (1980)
- (Ba 60) Bankoff, S.G.:
A Variable Density Single-Fluid Model for
Two-Phase with Particular Reference to
Steam-Water Flow
J. Heat Transfer 82 (C), 1960
- (Be et al. 80) Beraha, D., A. Hoeld, and Z. Jakubowski:
Multilevel Control of the Power Density
Distribution in a Nuclear Reactor Core
6th IFAC/IFIP Int. Conf. on Digital
Computer Applications to Process Control,
Düsseldorf, October 14-17, 1980
- (Be 83) Beraha, D.:
Multilevel Core Control System (MCCS)
for PWR Power Plants
To be published
- (Bu, He 77) Butterworth, D., and G.F. Hewitt:
Two Phase Flow and Heat Transfer
Oxford Univ. Press, 1977, S. 161-166
- (Er 80) Ercan, Y.:
A Model for Simulation of BWR Nuclear
Power Plants
(unpublished notes), 1980

- (Er et al. 82) Ercan, Y., A. Hoeld and O. Lupas:
GARLIC-B. A Digital Code for Real-Time
Calculation of the Transient Behaviour
of Nodal and Global Core and Plant Para-
meters of BWR Nuclear Power Plants.
Program Description.
GRS-39 (April 1982)
- (Fi, Fi 81) Fischer, H.D., and H. Finnemann:
The Nodal Integration Method - A Diverse
Solver for Neutron Diffusion Problems
ATKE 39 (1981), S. 176-183
- (Fi, Gu 81) Finnemann, H., and W. Gundlach:
Space-time Kinetics Code IQSBOX for PWR
and BWR. Part I: Description of Physical
and Thermohydraulic Models.
ATKE 37 (1981), S. 176-162
- (Ho et al. 81) Hoeld, A., Y. Ercan, O. Lupas and D. Beraha:
Status of the Core Surveillance Systems
at the GRS
EHPG-Meeting, Fredrikstad, June 14-19, 1981
- (Ho et al. 82) Hoeld, A., O. Lupas, V. Rossi, D. Henke and
K. Luger:
GARLIC. A Digital Code for the Real-Time
Calculation of the Operational Transient
Behaviour of Important Nodal and Global PWR
Core and Plant Parameters.
Program Description
Ed. GRS (Oktober 1982)
- (Ho, Lu 80) Hoeld, A., and O. Lupas:
GARLIC. A Real-Time Simulator for PWR Nuclear
Power Plants
EHPG-Meeting, Lillehammer, June 1-6, 1980

- (Ho, Lu 81) Hoeld, A., and O. Lupas:
Real-Time Simulation of the Transient Behaviour of Local and Global PWR Core and Plant Parameters.
Presented at the International Topical Meeting on Advances in Mathematical Methods for the Solution of Nuclear Engineering Problems, Munich, April 27-29, 1981
- (Ho, Lu 82) Hoeld, A., and O. Lupas:
A Nonlinear 3D Real-Time Model for PWR Nuclear Power Plants
Model Description
Ed. GRS (September 1982)
- (La et al. 77a) Langenbuch, S., W. Maurer and W. Werner:
Coarse-mesh Flux-expansion Method for the Analysis of Space-time Effects in Large Light Water Reactor Cores.
Nucl. Sci. and Eng. 63 (1977), S. 437-456
- (La et al. 77b) Langenbuch, S., W. Maurer and W. Werner:
High-Order Schemes for Neutron Kinetics Calculations, Based on a Local Polynomial Approximation
Nucl. Sci. and Eng. 64 (1977), S. 508-516
- (La et al. 78) Langenbuch, S., W. Maurer and W. Werner:
QUABOX/CUBBOX - Version 02. Ein Grobgitterverfahren zur Lösung der Neutronendiffusionsgleichungen. Programmbeschreibung.
Ed. GRS (Juli 1978)
- (Lo et al. 81) Lockau, J., H. Eckey, H. Finnemann and
W. Gundlach:
Space-time Kinetics Code IQSBOX for PWR and BWR. Part II: Verification against Experiments and Application of Special Problems
ATKE 37 (1981), S. 249-256

- (Ma, Ne 48) Martinelli, R.C., and D.B. Nelson:
Prediction of Pressure Drop during Forced-
Circulation of Boiling Water
Trans. ASME 70, August 1948, S. 695-702
- (Mo 48) Moody, L.F.:
Friction Factors for Pipe Flow
Trans. ASME 66, November 1948, S. 671 (see
also: VDI-Wärmeatlas, LB1, 1963)
- (Sa, Zu 74) Saha, P., and N. Zuber:
Point of Net Vapor Generation and Vapor Void
Fraction in Subcooled Boiling
5th Int. Heat Transfer Conference,
Tokyo, 1974
- (Si 76) Siewers, H.:
An Efficient Coarse Mesh Rebalancing Method
for Nodal Cores
ATKE 28 (1976), S. 1975-1978

APPENDIXES

Appendix 1THE POWER FEEDBACK COEFFICIENTS FROM THE COOLANT TEMPERATURE TERMS

The coefficients Λ_{nj} in equation (5.2) are defined as follows:

A1.1 Channels without Border Zone

- Nodes with Single Phase Flow ($n=(k-1)n_z+1, \dots, (k-1)n_z+n_{dk}$)
For $n = (k-1)n_z+1$:

$$\Lambda_{nj} = 0 \quad (j \neq n)$$

$$\Lambda_{nj} = \frac{P_N V_n}{2T_{CN} h_w^T G_{kw}} \quad (j = n)$$

For $n > (k-1)n_z+1$:

$$\Lambda_{nj} = \frac{P_N V_j}{T_{CN} h_w^T G_{kw}} \quad \text{for} \quad (k-1)n_z+1 \leq j \leq n-1$$

$$\Lambda_{nj} = \frac{P_N V_j}{2T_{CN} h_w^T G_{kw}} \quad (j = n)$$

$$\Lambda_{nj} = 0 \quad (j = n+1)$$

- Nodes with Subcooled Boiling

a) Node with Bubble Detachment Point ($n=(k-1)n_z+n_{dk}+1$)

- without boiling boundary:

if $n_{dk} = 0$:

$$\Lambda_{nj} = 0 \quad \text{for} \quad (k-1)n_z + 1 \leq j \leq n-1$$

$$\Lambda_{nj} = \frac{I_{Bn} P_N}{\Delta z_n T_{CN}} \quad (j = n)$$

$$\Lambda_{nj} = 0 \quad (j = n+1)$$

if $n_{dk} \neq 0$:

$$\Lambda_{nj} = \frac{\Delta z_{dkw} V_j P_N}{2\Delta z_n h_w^T G_{kw} T_{CN}} \quad \text{for} \quad (k-1)n_z + 1 \leq j \leq n-1$$

$$\Lambda_{nj} = \frac{I_{Bn} P_N}{\Delta z_n T_{CN}} \quad (j = n)$$

$$\Lambda_{nj} = 0 \quad (j = n+1)$$

- with boiling boundary:

if $n_{dk} = 0$:

$$\Lambda_{nj} = 0 \quad \text{for} \quad (k-1)n_z + 1 \leq j \leq n-1$$

$$\Lambda_{nj} = \frac{I'_{Bn} P_N}{\Delta z_n T_{CN}} \quad (j = n)$$

$$\Lambda_{nj} = 0 \quad (j = n+1)$$

if $n_{dk} \neq 0$:

$$\Lambda_{nj} = \frac{\Delta z_{dkw} V_j P_N}{2\Delta z_n h_w^T G_{kw} T_{CN}} \quad \text{for} \quad (k-1)n_z + 1 \leq j \leq n-1$$

$$\Lambda_{nj} = \frac{I'_{Bn} P_N}{\Delta z_n T_{CN}} \quad (j = n)$$

$$\Lambda_{nj} = 0 \quad (j = n+1)$$

b) Node without Bubble Detachment Point ($n > (k-1)n_z + n_{dk} + 1$)

- without boiling boundary:

$$\Lambda_{nj} = \frac{P_N I_{Bj}}{\Delta z_n T_{CN}} \quad \text{for } (k-1)n_z + n_{dk} + 1 \leq j \leq n-1$$

$$\Lambda_{nj} = \frac{P_N I_{Bn}}{\Delta z_n T_{CN}} \quad (j = n)$$

$$\Lambda_{nj} = 0 \quad (j = n+1)$$

- with boiling boundary:

$$\Lambda_{nj} = \frac{P_N I'_{Bj}}{T_{CN} \Delta z_n} \quad \text{for } (k-1)n_z + n_{dk} + 1 \leq j \leq n-1$$

$$\Lambda_{nj} = \frac{P_N I'_{Bn}}{\Delta z_n T_{CN}} \quad (j = n)$$

$$\Lambda_{nj} = 0 \quad (j = n+1)$$

● Nodes with Normal Boiling

$$\Lambda_{nj} = 0 \quad \text{for } (k-1)n_z + 1 \leq j \leq n+1$$

I_{Bn} , I'_{Bn} , I_{Bj} and I'_{Bj} in the above expressions are integral terms whose definitions are given in (Er 80).

A1.2 Channels with Border Zone

The coolant temperature-power feedback terms from the nodes which lie on a channel with a border zone can also be expressed as in equation (5.2). However, calculations of the coefficients Λ_{nj} are tedious and many numerical integrations are needed. Detailed expressions for Λ_{nj} are found in (Er 80).

Appendix 2THE POWER FEEDBACK COEFFICIENTS FROM THE VOID FRACTION TERMS

The coefficients W_{nj} in equation (5.14) are defined as follows:

A2.1 Channels without Border Zone

- Node with Bubble Detachment Point ($n=(k-1)n_z+n_{dk}+1$)

$$W_{nj} = 0 \quad (n \neq j)$$

$$W_{nj} = \frac{P_N D_{Bw}}{\alpha_N} \left(1 - \frac{\Delta z_{dkw}}{\Delta z_n}\right) z_{BM} \quad (n = j)$$

- Boiling Nodes without Bubble Detachment Point

$$W_{nj} = \frac{D_{nw} U_j I_{u1} P_N}{\alpha_N \Delta z_n} \quad \text{for } (k-1)n_z + n_{dk} + 1 \leq j \leq n-1$$

$$W_{nj} = \frac{V_n D_{nw} I_{u2} P_N}{\alpha_N h_{sw} G_{kw} (\Delta z_n)^2} \quad (j = n)$$

$$W_{nj} = 0 \quad (j = n+1)$$

Definitions of the terms D_{Bw} , D_{nw} , I_{u1} , I_{u2} and z_{BM} in the above expressions are given in (Er 80).

A2.2 Channels with Border Zone

The void fraction-power feedback terms from the nodes which lie on a channel with a border zone can also be expressed as in eq. (5.14). However, calculations of the coefficients W_{nj} are more tedious. Detailed expressions for W_{nj} are found in (Er 80).

**Gesellschaft für Anlagen-
und Reaktorsicherheit
(GRS)mbH**

Schwertnergasse 1
50667 Köln
Telefon (02 21) 20 68-0
Telefax (02 21) 20 68-888

Forschungsgelände
85748 Garching b. München
Telefon (0 89) 3 20 04-0
Telefax (0 89) 3 20 04-599

Kurfürstendamm 200
10719 Berlin
Telefon (0 30) 8 85 89-0
Telefax (0 30) 8 85 89-111

Theodor-Heuss-Straße 4
38122 Braunschweig
Telefon (0531) 80 12-0
Telefax (0531) 80 12-200